Numer. Math. (1999) 82: 433–470

Numerische Mathematik

Electronic Edition

A posteriori error analysis for numerical approximations of Friedrichs systems

P. Houston[1,⋆], **J.A. Mackenzie**[2], **E. Süli**[1], **G. Warnecke**[3,⋆]

[1] Oxford University Computing Laboratory, Wolfson Building, Parks Road, Oxford OX1 3QD, UK
[2] Department of Mathematics, University of Strathclyde, Glasgow, UK
[3] Institut für Analysis und Numerik, Otto-von-Guericke-Universität, Magdeburg, Germany

Received January 10, 1997 / Revised version received March 5, 1998

Summary. The global error of numerical approximations for symmetric positive systems in the sense of Friedrichs is decomposed into a locally created part and a propagating component. Residual-based two-sided local a posteriori error bounds are derived for the locally created part of the global error. These suggest taking the L^2-norm as well as weaker, dual norms of the computable residual as local error indicators. The dual graph norm of the residual $\boldsymbol{r}_h$ is further bounded from above and below in terms of the L^2 norm of $h\boldsymbol{r}_h$ where h is the local mesh size. The theoretical results are illustrated by a series of numerical experiments.

Mathematics Subject Classification (1991): 65M15, 65M50, 65M60

1. Introduction

One of the main challenges in the field of computational fluid dynamics concerns the accurate and efficient numerical solution of partial differential equations for complex multi-dimensional problems. Recent intensive research into this area has focused on the construction of reliable and robust algorithms which can deliver solutions with guaranteed error control. While for partial differential equations of solid mechanics several finite element packages exist which go quite a way towards achieving this goal, for

⋆ The work of Gerald Warnecke was partially supported by the Deutsche Forschungsgemeinschaft (Grant DFG Wa 633/4–1). Paul Houston acknowledges the financial support of the EPSRC (Grant GR/K76221).
Correspondence to: E. Süli

fluid flow problems the situation is far less advanced. Indeed, the majority of adaptive CFD algorithms will simply refine or adjust the computational mesh according to an ad hoc criterion, such as a large gradient in a physical quantity. Although this intuitive approach has had some success, it does not provide guaranteed error control. An alternative to this heuristic method is to derive reliable and efficient a posteriori error estimates which can successfully drive adaptive algorithms; indeed, our aim in this paper is to initiate the development of a theoretical framework for equations of compressible transonic gas dynamics. One of the key technical difficulties in accomplishing this task stems from the fact that the partial differential equations which govern the flow are nonlinear and, typically, of changing type (e.g. elliptic-hyperbolic); see [6].

The late 1950's witnessed an upsurge of research into the well-posedness of linearised transonic flow problems. A particularly useful family of linear partial differential equations which emerged from this study is that of symmetric positive systems in the sense of Friedrichs. This broad class includes, for example, first-order symmetric elliptic and hyperbolic systems as well as various equations of mixed type, and, therefore, it provides a natural starting point in developing a theoretical framework for reliable and robust adaptive transonic flow algorithms. This paper is concerned with the a posteriori error analysis of a general class of numerical methods for symmetric positive systems in the sense of Friedrichs.

We begin, in Sect. 2, by introducing the necessary notation and recall the basic theory of symmetric positive systems. In order to carry out a rigorous a posteriori error analysis we extend the original theory of symmetric systems developed by Friedrichs [5], Lax and Phillips [15]. In particular we define the graph space of a Friedrichs operator equipped with the associated *graph norm*, we prove trace theorems for this space, as well as associated integration-by-parts formulae.

The a posteriori error analysis performed in Sect. 3 relies on the stability of the boundary value problem for a Friedrichs system which we establish via Gårding's inequality. Next, we define the general class of numerical schemes to be considered and, exploiting the theory from Sect. 2, we provide two-sided residual-based global a posteriori error bounds on the graph-norm and the L^2 norm of the error in terms of the L^2 norm and the dual graph-norm of the residual, respectively. Obtaining local error estimates is one of the main technical difficulties in the a posteriori error analysis of discretisation methods for hyperbolic problems. We describe how this can be achieved by splitting the global error into a locally generated component, which we call the *cell error*, and a non-local part, called the *transmitted error*, which represents the accumulation of errors generated outside a cell and merely advected into it (see also [17, 18, 20]). Using this decomposition

and proceeding analogously as in the global analysis we obtain local error bounds in strong and weak norms. Thus we deduce that specific norms of the residual provide reliable and efficient bounds on associated norms of the cell error. These results indicate that the local residual contains information only about the error that has been created on an individual cell, which, in turn justifies the use of residual-based error indicators for adaptive local mesh refinement. The concept of cell error is a generalisation of that of the local error frequently used in a priori analysis of numerical methods for ordinary differential equations, see Sect. II.8 in [7]; it seems that it was not used in connection with a posteriori analysis of approximations to partial differential equations prior to [18].

Although the dual graph norm is a natural quantity to consider from the point of view of the error analysis, its definition makes it unsuitable for practical implementations and is difficult to localise. A key result in Sect. 4 is that the dual graph norm can be replaced by a quantity that is essentially equivalent to it and is easy to compute; in particular, we show that the dual graph norm of the residual can be further bounded from above by a constant multiple of $h_\kappa \|\boldsymbol{r}_h\|_{L_2(\kappa)}$, where h_κ is the diameter of κ. We shall also show that a similar lower bound holds, and thereby we deduce the following two-sided bound on the locally created component of the error in terms of the local residual:

$$c_2(\kappa)\|h_0 P_{h_0}\boldsymbol{r}_h\|_{L_2(\kappa)} \leq \|\boldsymbol{e}_\kappa^{\mathrm{cell}}\|_{L_2(\kappa)} \leq c_3(\kappa)\|h\boldsymbol{r}_h\|_{L_2(\kappa)}, \tag{1.1}$$

where c_2 and c_3 are positive constants, P_{h_0} is the orthogonal projector in $L_2(\kappa)$ onto a finite element subspace $S^{h_0} = S^{h_0}(\kappa) \subset L_2(\kappa)$ on a micropartition of κ of granularity h_0. Thus we arrive at a two-sided a posteriori bound that is simple to implement into adaptive algorithms.

We note that, for finite element approximations of scalar hyperbolic equations, non-local a posteriori error bounds on the transmitted error were derived in [30] (see also Remark 3.6 below) by exploiting the Galerkin orthogonality of the finite element method, together with the stability of the corresponding dual or adjoint problem, cf. [31]. Thus, unlike the a posteriori estimates discussed here, those bounds on the transmitted error are dependent on the particular discretisation employed.

In Sect. 5, we discuss the numerical implementation of these theoretical results and highlight the potentials of our a posteriori error bounds. The application of the theoretical framework developed here to the Euler equations of compressible gas dynamics is discussed in [24].

Seminal work in the area of residual-based a posteriori error analysis and adaptivity for Galerkin finite element approximations of linear elliptic equations has been carried out in [2] and [22], while for hyperbolic and almost-hyperbolic problems work in this area has been pursued in recent

years by Johnson and collaborators (see [9–11, 13], and references therein). The theoretical framework of a posteriori error estimation for Galerkin approximations of hyperbolic problems developed in the latter papers is based on an elliptic or parabolic regularisation of the hyperbolic partial differential equation through the addition of a mesh-dependent artificial viscosity term. The a posteriori error estimates are then derived by exploiting the strong stability of the adjoint to the regularised problem and the orthogonality of the residual to the Galerkin test space. This differs from our approach, in that we make no use of Galerkin orthogonality or artificial viscosity; indeed, our estimates are applicable to a general class of numerical schemes, including ones that lie outside the Galerkin framework, and also to methods which do not introduce artificial viscosity terms in an explicit fashion. Connections between the theory developed here and that of Johnson are discussed in more detail in [29] and [31].

This paper is an extended version of our note [18] and the conference paper [29].

2. Friedrichs systems

Let Ω be a bounded open set in $\mathbb{R}^n$ with a Lipschitz-continuous boundary; such a set will be called a *Lipschitz domain* (see Nečas [21]). We use $(\cdot,\cdot)$ to denote the L^2 inner product on Ω, and $\|\cdot\|_0$ for the corresponding L^2 norm on Ω; analogously, if Ω' is a measurable set contained in $\overline{\Omega}$, we denote by $(\cdot,\cdot)_{\Omega'}$ the L^2 inner product on Ω' and by $\|\cdot\|_{0,\Omega'}$ the associated L^2 norm. Similarly, any other norm will be indexed with a set provided it is taken over a proper subset of Ω; otherwise the reference to the domain will be omitted. The standard hilbertian Sobolev space on Ω of real order s will be denoted $H^s(\Omega)$, and the associated Sobolev norm will be labelled $\|\cdot\|_s$ (see Adams [1] for more details). We shall be using vector-valued functions $\boldsymbol{u}, \boldsymbol{v} : \Omega \to \mathbb{R}^m$. For such functions, denoting by $|\cdot|$ the Euclidean norm of $\mathbb{R}^m$, we set

$$(\boldsymbol{u},\boldsymbol{v}) := \sum_{j=1}^{m}(u_j, v_j), \quad \text{and} \quad \|\boldsymbol{u}\| := \||\boldsymbol{u}|\|$$

for any of the above scalar norms.

2.1. General theory of symmetric positive systems

We review here some basic results from the theory of symmetric systems in the sense of Friedrichs [5], see also Lax [14]. Suppose that we are given matrix-valued functions $A_i, C : \overline{\Omega} \to \mathbb{R}^{m\times m}$, $i = 1,\ldots,n$, and, for $k \in \mathbb{N}$,

the vector $\boldsymbol{f} \in [H^k(\Omega)]^m$. We assume that the components $(a^i_{jk})_{1\le j,k\le m}$ of the matrices A_i are in $C^1(\overline{\Omega})$ and the components $(c_{jk})_{1\le j,k\le m}$ of the matrix C are in $C(\overline{\Omega})$. We consider the system of first-order linear partial differential equations

$$L\boldsymbol{u} := \sum_{i=1}^{n} A_i \boldsymbol{u}_{x_i} + C\boldsymbol{u} = \boldsymbol{f} \qquad \text{on } \Omega, \tag{2.2}$$

and denote by L^* the *formal adjoint* of the operator L, defined by

$$L^*\boldsymbol{u} := -\sum_{i=1}^{n} \frac{\partial}{\partial x_i}\,(A_i^*\boldsymbol{u}) + C^*\boldsymbol{u}. \tag{2.3}$$

Following Friedrichs [5], the system (2.2) is said to be *symmetric positive* if the following conditions hold:

(1) the matrices A_i, for $i = 1, \ldots, n$, are symmetric, i.e. $A_i = A_i^*$;
(2) there exist $\alpha \ge 0$ and $\xi \in \mathbb{R}^n$, with $|\xi| = 1$, such that the symmetric part of the matrix

$$K_\xi := C - \frac{1}{2}\sum_{i=1}^{n} \frac{\partial}{\partial x_i} A_i + \alpha \sum_{i=1}^{n} \xi_i A_i$$

is positive definite, uniformly on $\overline{\Omega}$, i.e. there exists a positive constant $c_0 = c_0(\Omega)$ such that

$$\frac{1}{2}\left(K_\xi(x) + K_\xi^*(x)\right) \ge c_0 I \tag{2.4}$$

for all x in $\overline{\Omega}$. For simplicity, we shall often write K instead of K_ξ.

The system (2.2) will be called *dissipative* if (2.4) holds for $\alpha = 0$. We note that a sufficient condition for (2.4) to hold is that:

(2') there exists $\xi \in \mathbb{R}^n$, with $|\xi| = 1$, and a positive constant $c_0' = c_0'(\Omega)$, such that

$$\xi_1 A_1(x) + \ldots + \xi_n A_n(x) \ge c_0' I,$$

for all $x \in \overline{\Omega}$.

In this case, ξ is called a time-like direction, and the hyperplane to which $\xi = (\xi_1, \ldots, \xi_n)$ is normal at the point x is called a space-like hyperplane at x. An important special case when (2') (and thereby (2)) is trivially satisfied is when at least one of the A_i is positive definite, uniformly on $\overline{\Omega}$. Condition (2') will not be made use of until Sect. 4; there we shall assume that (2') holds, instead of (2).

On the boundary, $\partial\Omega$, the unit outer normal vector field $\hat{\nu} = (\hat{\nu}_1, \ldots, \hat{\nu}_n)$ is defined almost everywhere with respect to the $(n-1)$-dimensional measure on $\partial\Omega$. Consider the matrix

$$B := \sum_{i=1}^{n} \hat{\nu}_i A_i. \tag{2.5}$$

For the sake of simplicity we shall assume that B is non-singular almost everywhere on $\partial\Omega$, that is, the boundary of Ω is nowhere characteristic. This can be seen as an assumption either on the system or on the domain Ω.

We denote by B^- the negative part of the symmetric matrix B; thus B^- is negative semi-definite and $B^+ = B - B^-$ is positive semi-definite. Given that $\boldsymbol{g}$ belongs to $[H^{k+1}(\Omega)]^m$, $k \geq 0$, the trace $\Gamma_{0,\partial\Omega}\boldsymbol{g}$ of $\boldsymbol{g}$ in $[H^{k+\frac{1}{2}}(\partial\Omega)]^m$ defines an admissible boundary condition via

$$B^-\boldsymbol{u} = B^-\boldsymbol{g} \quad \text{on } \partial\Omega. \tag{2.6}$$

Suppose that we are given $\boldsymbol{f} \in [H^1(\Omega)]^m$ and $\boldsymbol{g} \in [H^1(\partial\Omega)]^m$; then there exists a unique solution $\boldsymbol{u} \in [H^1(\Omega)]^m$ of the boundary value problem (2.2), (2.6) such that

$$\|\boldsymbol{u}\|_k \leq c(\|\boldsymbol{f}\|_k + \|\boldsymbol{g}\|_{k,\partial\Omega}) \tag{2.7}$$

for $k = 0, 1$ (see Friedrichs [5], Lax [14], Lax–Phillips [15] and Taylor [32, Chapter IV].) We remark here that a precise definition of *solution* will be given in Sect. 2.3, following the discussion on the graph space of the operator L in Sect. 2.2. Note that, by linearity, we may use a standard argument to ensure that $\boldsymbol{g} \equiv \boldsymbol{0}$, at the expense of modifying $\boldsymbol{f}$.

2.2. The graph space

In the following we introduce the basic ingredients for our a posteriori error analysis of numerical schemes for Friedrichs systems. First, we define the *graph space* on Ω corresponding to the operator L:

$$H(L, \Omega) := \{\boldsymbol{u} \in [L^2(\Omega)]^m \mid L\boldsymbol{u} \in [L^2(\Omega)]^m\}.$$

Note that $[H^1(\Omega)]^m$ is contained in $H(L, \Omega)$. Using α and ξ as in the definition of the matrix $K = K_\xi$ in condition (2), we introduce on $H(L, \Omega)$ the *weighted graph norm*

$$|||\boldsymbol{u}||| := \left(\|\mathrm{e}^{-\alpha(\xi\cdot x)}\boldsymbol{u}\|_0^2 + \|\mathrm{e}^{-\alpha(\xi\cdot x)}L\boldsymbol{u}\|_0^2\right)^{1/2}.$$

Next we state and prove a trace theorem for the space $H(L, \Omega)$ and give an associated integration-by-parts formula. We shall denote the duality pairing

between the Sobolev space $[H^{\frac{1}{2}}(\partial\Omega)]^m$ and its dual space by $\langle\cdot,\cdot\rangle_{\partial\Omega}$, and by $\Gamma_{0,\partial\Omega} : [H^1(\Omega)]^m \to [H^{\frac{1}{2}}(\partial\Omega)]^m$ the usual trace operator (see Nečas [21]). The L^2 inner product on $\partial\Omega$ will be denoted $(\cdot,\cdot)_{\partial\Omega}$.

Theorem 2.1 **(**Trace Theorem) *Let $\Omega \subset \mathbb{R}^n$ be a Lipschitz domain. There exists a bounded linear* trace operator

$$\Gamma_{B,\partial\Omega} : H(L,\Omega) \to \left([H^{\frac{1}{2}}(\partial\Omega)]^m\right)'$$

such that, for any $\boldsymbol{u}$ in $[H^1(\Omega)]^m$,

$$\Gamma_{B,\partial\Omega}\boldsymbol{u} = B\left(\Gamma_{0,\partial\Omega}\boldsymbol{u}\right). \tag{2.8}$$

In addition, the following integration-by-parts formula holds for all $\boldsymbol{u}$ in $H(L,\Omega)$ and all $\boldsymbol{w}$ in $[H^1(\Omega)]^m$:

$$\begin{aligned}\sum_{i=1}^{n}\int_\Omega (A_i\boldsymbol{u}_{x_i})\cdot\boldsymbol{w}\,dx = -\sum_{i=1}^{n}\int_\Omega \boldsymbol{u}\cdot(A_i\boldsymbol{w})_{x_i}\,dx \\ +\langle\Gamma_{B,\partial\Omega}\boldsymbol{u},\Gamma_{0,\partial\Omega}\boldsymbol{w}\rangle_{\partial\Omega}.\end{aligned} \tag{2.9}$$

Proof. Given that $\boldsymbol{g} \in [H^{1/2}(\partial\Omega)]^m$, consider any $\boldsymbol{w}$ in $[H^1(\Omega)]^m$ such that $\boldsymbol{g} = \Gamma_{0,\partial\Omega}\boldsymbol{w}$. We set, for $\boldsymbol{u}$ in $H(L,\Omega)$,

$$F_{\boldsymbol{u}}(\boldsymbol{g}) = \sum_{i=1}^{n}\int_\Omega \left[(A_i\boldsymbol{u}_{x_i})\cdot\boldsymbol{w} + \boldsymbol{u}\cdot(A_i\boldsymbol{w})_{x_i}\right]dx, \tag{2.10}$$

which defines a linear functional on $[H^{\frac{1}{2}}(\partial\Omega)]^m$. It is easily shown that the definition of $F_{\boldsymbol{u}}(\boldsymbol{g})$ is independent of the choice of $\boldsymbol{w}$, with $\Gamma_{0,\partial\Omega}\boldsymbol{w} = \boldsymbol{g}$. Applying the Cauchy-Schwarz inequality, and denoting by $\tilde{c}$ a suitable positive constant,

$$|F_{\boldsymbol{u}}(\boldsymbol{g})| \le \tilde{c}|||\boldsymbol{u}|||\cdot\|\boldsymbol{w}\|_1. \tag{2.11}$$

According to Nečas [21, Sect. 2.5.7], there exists a continuous linear extension operator $T : [H^{\frac{1}{2}}(\partial\Omega)]^m \to [H^1(\Omega)]^m$. Therefore, with $\boldsymbol{w} = T\boldsymbol{g}$ and a suitable positive constant c_1, we have that

$$|F_{\boldsymbol{u}}(\boldsymbol{g})| \le \tilde{c}|||\boldsymbol{u}|||\cdot\|\boldsymbol{w}\|_1 \le c_1|||\boldsymbol{u}|||\cdot\|\boldsymbol{g}\|_{\frac{1}{2},\partial\Omega}; \tag{2.12}$$

hence $F_{\boldsymbol{u}}$ belongs to $\left([H^{\frac{1}{2}}(\partial\Omega)]^m\right)'$. We set $\Gamma_{B,\partial\Omega}\boldsymbol{u} := F_{\boldsymbol{u}}$. Due to (2.12) the linear operator

$$\Gamma_{B,\partial\Omega} : H(L,\Omega) \to \left([H^{\frac{1}{2}}(\partial\Omega)]^m\right)'$$

is continuous. Now (2.10) implies (2.9) since

$$F_u(\boldsymbol{g}) = \langle \Gamma_{B,\partial\Omega}\boldsymbol{u}, \Gamma_{0,\partial\Omega}\boldsymbol{w}\rangle_{\partial\Omega}.$$

Consider $\boldsymbol{u}$ in $[C^1(\overline{\Omega})]^m$ and let $\boldsymbol{w}$ belong to $[C^1(\overline{\Omega})]^m$. Thence, using (2.10) and Gauss' theorem, we get

$$\langle \Gamma_{B,\partial\Omega}\boldsymbol{u}, \boldsymbol{g}\rangle_{\partial\Omega} = F_{\boldsymbol{u}}(\boldsymbol{g}) = \sum_{i=1}^{n} \int_\Omega \left[A_i\boldsymbol{u}\cdot\boldsymbol{w}\right]_{x_i}\, dx = \int_{\partial\Omega} (B\boldsymbol{u})\cdot\boldsymbol{g}\, dS.$$

This implies (2.8) for all $\mathbf{u}$ in $[C^1(\overline{\Omega})]^m$. Since $[C^1(\overline{\Omega})]^m$ is dense in $H(L,\Omega)$ we deduce that

$$\Gamma_{B,\partial\Omega}\boldsymbol{u} = B\left(\Gamma_{0,\partial\Omega}\boldsymbol{u}\right). \quad \square$$

Let us consider the adjoint operator L^* given by (2.3), and the associated graph space $H(L^*,\Omega)$ equipped with the norm

$$|||\boldsymbol{u}|||_* := \left(\|\mathrm{e}^{\alpha(\xi\cdot x)}\boldsymbol{u}\|_0^2 + \|\mathrm{e}^{\alpha(\xi\cdot x)}L^*\boldsymbol{u}\|_0^2\right)^{1/2}.$$

Then, in analogy with Theorem 2.1, we have the following result.

Theorem 2.2 (Dual Trace Theorem) *Let Ω be Lipschitz domain in $\mathbb{R}^n$. There exists a bounded linear* trace operator

$$\Gamma^*_{B,\partial\Omega} : H(L^*,\Omega) \to \left([H^{\frac{1}{2}}(\partial\Omega)]^m\right)',$$

such that, for any $\boldsymbol{w}$ in $[H^1(\Omega)]^m$,

$$\Gamma^*_{B,\partial\Omega}\boldsymbol{w} = \Gamma_{B,\partial\Omega}\boldsymbol{w} = B\left(\Gamma_{0,\partial\Omega}\boldsymbol{w}\right). \tag{2.13}$$

For all $\boldsymbol{w} \in H(L^*,\Omega)$ and all $\boldsymbol{u} \in [H^1(\Omega)]^m$ we have the following integration-by-parts formula:

$$\sum_{i=1}^{n} \int_\Omega \boldsymbol{u}\cdot\left(A_i\boldsymbol{w}\right)_{x_i}\, dx = -\sum_{i=1}^{n} \int_\Omega \left(A_i\boldsymbol{u}_{x_i}\right)\cdot\boldsymbol{w}\, dx + \langle \Gamma_{0,\partial\Omega}\boldsymbol{u}, \Gamma^*_{B,\partial\Omega}\boldsymbol{w}\rangle_{\partial\Omega}.$$

Proof. The proof is analogous to that of the preceding theorem. $\square$

The splitting $B = B^+ + B^-$ induces a natural decomposition of the trace operator $\Gamma_{B,\partial\Omega}$ which leads us to define the partial trace operators

$$\Gamma_{B^\pm,\partial\Omega} : H(L,\Omega) \to \left([H^{\frac{1}{2}}(\partial\Omega)]^m\right)'$$

with

$$\Gamma_{B,\partial\Omega} = \Gamma_{B^+,\partial\Omega} + \Gamma_{B^-,\partial\Omega}.$$

By virtue of the formula (2.8), on the dense subset $[H^1(\Omega)]^m$ of $H(L,\Omega)$ this decomposition can be constructed by splitting the trace of $\boldsymbol{u} \in [H^1(\Omega)]^m$ and then extending the operators by continuity to all of $H(L,\Omega)$. One can proceed analogously for $H(L^*,\Omega)$.

Now we are ready to precisely define the domains of the operators L and L^*: the domain of definition of L is

$$D(L,\Omega) = \{\boldsymbol{u} \in [L^2(\Omega)]^m \mid L\boldsymbol{u} \in [L^2(\Omega)]^m \text{ and } \Gamma_{B^-,\partial\Omega}\boldsymbol{u} = \boldsymbol{0}\}$$

and that of L^* is defined by

$$D(L^*,\Omega) = \{\boldsymbol{u} \in [L^2(\Omega)]^m \mid L^*\boldsymbol{u} \in [L^2(\Omega)]^m \text{ and } \Gamma_{B^+,\partial\Omega}\boldsymbol{u} = \boldsymbol{0}\}.$$

With the (weighted) graph norms $|||\cdot|||$, respectively $|||\cdot|||_*$, defined above, the domain $D(L,\Omega)$, respectively $D(L^*,\Omega)$, is a subspace of the Hilbert space $H(L,\Omega)$, respectively $H(L^*,\Omega)$.

Lemma 2.3 *Let κ be a Lipschitz subdomain of Ω. Given any $\boldsymbol{u}$ in $D(L,\kappa)$ and $\boldsymbol{w}$ in $D(L^*,\kappa)$, we have that*

$$(L\boldsymbol{u},\boldsymbol{w})_\kappa = (\boldsymbol{u},L^*\boldsymbol{w})_\kappa. \tag{2.14}$$

Proof. The equality (2.14) obviously holds for $\boldsymbol{u}$ in the dense subset $D(L,\kappa) \cap C^1(\overline{\kappa})$ of $D(L,\kappa)$ and $\boldsymbol{w}$ in the dense subset $D(L^*,\kappa) \cap C^1(\overline{\kappa})$ of $D(L^*,\kappa)$. The desired result follows by continuity. □

2.3. Weak and strong solutions

Suppose that $\boldsymbol{f} \in [L^2(\Omega)]^m$, $\boldsymbol{g} \in [L^2(\partial\Omega)]^m$. A function $\boldsymbol{u} \in [L^2(\Omega)]^m$ satisfying

$$(\boldsymbol{u},L^*\boldsymbol{\varphi}) + \langle B^-\boldsymbol{g},\boldsymbol{\varphi}\rangle_{\partial\Omega} = (\boldsymbol{f},\boldsymbol{\varphi}), \tag{2.15}$$

for all $\boldsymbol{\varphi} \in D(L^*,\Omega)$ is called a *weak solution* of the boundary value problem (2.2), (2.6).

A weak solution $\boldsymbol{u}$ that belongs to $H(L,\Omega)$ is called a *strong solution*. Lax and Phillips [15] proved, under the assumption that B is non-singular, that every weak solution is a strong solution, and hence any weak solution is a solution of the boundary value problem

$$L\boldsymbol{u} = \boldsymbol{f} \quad \text{a.e. on } \Omega, \qquad \Gamma_{B^-,\partial\Omega}\boldsymbol{u} = B^-\boldsymbol{g} \quad \text{a.e. on } \partial\Omega.$$

The fact that $\boldsymbol{u} \in H(L,\Omega)$ does not preclude the possibility of $\boldsymbol{u}$ being discontinuous. The derivatives appearing in $L\boldsymbol{u}$ in the definition of $H(L,\Omega)$ are interior derivatives along characteristic hyper-surfaces and therefore $L\boldsymbol{u}$ will belong to $L^2(\Omega)$, even if $\boldsymbol{u}$ has a discontinuity across a characteristic hypersurface.

3. A posteriori error analysis

An important ingredient in the a posteriori error analysis presented here is a version of Gårding's inequality given below. Using this, we derive global and local bounds on the discretisation error.

For the sake of simplicity, throughout Sects. 3.1 and 3.2, we shall assume that $\alpha = 0$. Note that if the symmetric part of K is non-positive on $\overline{\Omega}$ for $\alpha = 0$ then the system can be transformed into one that is dissipative in the following way. Suppose that we set, for $\beta \in \mathbb{R}$,

$$\boldsymbol{u}(x) = \mathrm{e}^{\beta(\xi \cdot x)} \boldsymbol{v}(x);$$

then we obtain, for strong solutions, the equivalent system

$$L\boldsymbol{v} + \beta \sum_{i=1}^{n} \xi_i A_i \boldsymbol{v} = \mathrm{e}^{-\beta(\xi \cdot x)} \boldsymbol{f}$$

with

$$K = \left(C + \beta \sum_{i=1}^{n} \xi_i A_i \right) - \frac{1}{2} \sum_{i=1}^{n} \frac{\partial}{\partial x_i} A_i.$$

Now redefining the matrix C as the expression in the brackets, for β large enough, we obtain a new system which satisfies condition (2) above with $\alpha = 0$.

3.1. Estimates for the Friedrichs system and its adjoint

With the system (2.2) we associate, for $\boldsymbol{u} \in H(L, \Omega)$ and $\boldsymbol{v} \in [L^2(\Omega)]^m$, the *bilinear form*

$$b[\boldsymbol{u}, \boldsymbol{v}] := (L\boldsymbol{u}, \boldsymbol{v}). \tag{3.16}$$

Suppose that $\boldsymbol{u} \in [C^1(\overline{\Omega})]^m$. Integrating by parts and exploiting the symmetry of the A_i gives, for $i = 1, \ldots, n$,

$$(A_i \boldsymbol{u}_{x_i}, \boldsymbol{u}) = -\frac{1}{2}(\left(\frac{\partial}{\partial x_i} A_i \right) \boldsymbol{u}, \boldsymbol{u}) \; + \frac{1}{2}(\hat{\nu}_i A_i \boldsymbol{u}, \boldsymbol{u})_{\partial\Omega} \tag{3.17}$$

and

$$(\frac{\partial}{\partial x_i} (A_i \boldsymbol{u}) \, , \boldsymbol{u}) = \frac{1}{2}(\left(\frac{\partial}{\partial x_i} A_i \right) \boldsymbol{u}, \boldsymbol{u}) + \frac{1}{2}(\hat{\nu}_i A_i \boldsymbol{u}, \boldsymbol{u})_{\partial\Omega}. \tag{3.18}$$

Summing over i yields

$$b[\boldsymbol{u}, \boldsymbol{u}] = (\left[C - \frac{1}{2} \left(\sum_{i=1}^{n} \frac{\partial}{\partial x_i} A_i \right) \right] \boldsymbol{u}, \boldsymbol{u}) + \frac{1}{2}(B\boldsymbol{u}, \boldsymbol{u})_{\partial\Omega}.$$

Using (2.4), (3.17) and (3.18) we deduce that

$$\begin{aligned} b[\boldsymbol{u},\boldsymbol{u}] &= \frac{1}{2}\Big((L\boldsymbol{u},\boldsymbol{u})+(\boldsymbol{u},L\boldsymbol{u})\Big) \\ &= \frac{1}{2}\Big((L\boldsymbol{u},\boldsymbol{u})+(L^*\boldsymbol{u},\boldsymbol{u})\Big)+\frac{1}{2}(B\boldsymbol{u},\boldsymbol{u})_{\partial\Omega} \\ &= \frac{1}{2}\sum_{i=1}^{n}\left((A_i\boldsymbol{u}_{x_i},\boldsymbol{u})-(\frac{\partial}{\partial x_i}\left(A_i\boldsymbol{u}\right),\boldsymbol{u})\right) \\ &\quad +\left(\frac{1}{2}\left(C+C^*\right)\boldsymbol{u},\boldsymbol{u}\right)+\frac{1}{2}(B\boldsymbol{u},\boldsymbol{u})_{\partial\Omega} \\ &= \frac{1}{2}((K+K^*)\,\boldsymbol{u},\boldsymbol{u})+\frac{1}{2}(B\boldsymbol{u},\boldsymbol{u})_{\partial\Omega} \\ &\geq c_0\|\boldsymbol{u}\|_0^2+\frac{1}{2}(B\boldsymbol{u},\boldsymbol{u})_{\partial\Omega}, \end{aligned} \tag{3.19}$$

and hence the *Gårding inequality*

$$b[\boldsymbol{u},\boldsymbol{u}] \geq c_0\|\boldsymbol{u}\|_0^2+\frac{1}{2}(B^-\boldsymbol{u},\boldsymbol{u})_{\partial\Omega} \tag{3.20}$$

for all $\boldsymbol{u}\in[C^1(\overline{\Omega})]^m$; since $[C^1(\overline{\Omega})]^m$ is dense in $[H^1(\Omega)]^m$, we deduce that (3.20) holds for all $\boldsymbol{u}\in[H^1(\Omega)]^m$. In particular for all $\boldsymbol{u}$ in $[C^1(\overline{\Omega})]^m\cap D(L,\Omega)$,

$$b[\boldsymbol{u},\boldsymbol{u}] \geq c_0\|\boldsymbol{u}\|_0^2.$$

Since $[C^1(\overline{\Omega})]^m\cap D(L,\Omega)$ is dense in $D(L,\Omega)$ the coercivity of $b[\cdot,\cdot]$ follows:

$$b[\boldsymbol{u},\boldsymbol{u}] \geq c_0\|\boldsymbol{u}\|_0^2 \tag{3.21}$$

for all $\boldsymbol{u}\in D(L,\Omega)$. Exploiting this inequality we prove the following theorem.

Theorem 3.1 *For $\boldsymbol{u}\in D(L,\Omega)$ we have that*

$$\|\boldsymbol{u}\|_0 \leq \frac{1}{c_0}\|L\boldsymbol{u}\|_0 \tag{3.22}$$

and, with $c_1=(1+1/c_0^2)^{1/2}$ and $\alpha=0$, the following equivalence of norms:

$$\|L\boldsymbol{u}\|_0 \leq |||\boldsymbol{u}||| \leq c_1\|L\boldsymbol{u}\|_0. \tag{3.23}$$

Proof. Note that (3.21) implies that, for $\boldsymbol{u}\in D(L,\Omega)\subset[L^2(\Omega)]^m$,

$$\|L\boldsymbol{u}\|_0=\sup_{\boldsymbol{w}\in[L^2(\Omega)]^m}\frac{(L\boldsymbol{u},\boldsymbol{w})}{\|\boldsymbol{w}\|_0}\geq\frac{(L\boldsymbol{u},\boldsymbol{u})}{\|\boldsymbol{u}\|_0}=\frac{b[\boldsymbol{u},\boldsymbol{u}]}{\|\boldsymbol{u}\|_0}\geq c_0\|\boldsymbol{u}\|_0.$$

This in turn implies that

$$c_1\|L\boldsymbol{u}\|_0 \geq |||\boldsymbol{u}||| \tag{3.24}$$

and hence (3.23). □

For the purpose of deriving a posteriori error bounds in weaker norms we introduce the dual space $D'(L,\Omega)$ (respectively $D'(L^*,\Omega)$) to $D(L,\Omega)$ (respectively $D(L^*,\Omega)$) with the *dual (weighted) graph norm*

$$|||\boldsymbol{u}|||' := \sup_{\boldsymbol{v}\in D(L,\Omega)} \frac{(\boldsymbol{u},\boldsymbol{v})}{|||\boldsymbol{v}|||} \left(\text{respectively } |||\boldsymbol{u}|||'_* := \sup_{\boldsymbol{v}\in D(L^*,\Omega)} \frac{(\boldsymbol{u},\boldsymbol{v})}{|||\boldsymbol{v}|||_*}. \right)$$

Due to the continuous embeddings $[H_0^1(\Omega)]^m \subset D(L,\Omega) \subset [L^2(\Omega)]^m$, we have the dual embeddings $[L^2(\Omega)]^m \subset D'(L,\Omega) \subset [H^{-1}(\Omega)]^m$.

We consider, for $\boldsymbol{f} \in [H^1(\Omega)]^m$ and $\boldsymbol{g} \in [H^1(\partial\Omega)]^m$, the *adjoint boundary value problem*

$$\text{(3.25)} \qquad \begin{cases} L^*\boldsymbol{\varphi} \;= -\displaystyle\sum_{i=1}^{n} \frac{\partial}{\partial x_i}\,(A_i\boldsymbol{\varphi}) + C^*\boldsymbol{\varphi} = \boldsymbol{f} \quad \text{on } \Omega, \\ \\ B^+\boldsymbol{\varphi} = B^+\boldsymbol{g} \;\text{ on } \partial\Omega. \end{cases}$$

Writing the operator L^* as

$$L^*\boldsymbol{\varphi} = \sum_{i=1}^{n} A_i\boldsymbol{\varphi}_{x_i} + \sum_{i=1}^{n} \left(\frac{\partial}{\partial x_i} A_i \right) \boldsymbol{\varphi} + C^*\boldsymbol{\varphi}$$

one easily sees that this is again a symmetric positive system and all the results concerning L hold, by analogy, for the adjoint boundary value problem (3.25). We have the adjoint bilinear form

$$b^*[\boldsymbol{u},\boldsymbol{v}] := (\boldsymbol{u}, L^*\boldsymbol{v})$$

satisfying

$$b^*[\boldsymbol{u},\boldsymbol{u}] \geq c_0\|\boldsymbol{u}\|_0^2 - \frac{1}{2}(B\boldsymbol{u},\boldsymbol{u})_{\partial\Omega},$$

and the associated Gårding inequality

$$b^*[\boldsymbol{u},\boldsymbol{u}] \geq c_0\|\boldsymbol{u}\|_0^2 - \frac{1}{2}(B^+\boldsymbol{u},\boldsymbol{u})_{\partial\Omega},$$

for all $\boldsymbol{u} \in [H^1(\Omega)]^m$. In addition, similarly as for L, we have, for $\alpha = 0$ and any $\boldsymbol{u} \in D(L^*,\Omega)$,

$$\text{(3.26)} \qquad \|\boldsymbol{u}\|_0 \leq |||\boldsymbol{u}|||_* \leq c_1\|L^*\boldsymbol{u}\|_0 \leq c_1|||\boldsymbol{u}|||_*.$$

3.2. Global a posteriori error estimates

Consider the boundary value problem (2.2), (2.6) stated in Sect. 2. We wish to develop, in an abstract setting, the idea of error localisation and residual-based local a posteriori error estimation operating within the framework introduced below. Suppose that $\mathcal{U}^h \subset H(L,\Omega)$ is a finite element trial space obtained by partitioning Ω by a family consisting of N_h subsets $(\kappa_i)_{i=1,\ldots,N_h}$. The sets κ_i will be called *cells*. These could be, for example, triangles or quadrilaterals in the case $n=2$. For each cell we assume that it satisfies the same properties as the set Ω itself; thus all the analytical results proved in the case of Ω will also hold with Ω replaced by a cell κ_i. The mesh parameter h is defined to be the maximum diameter of the cells. We denote by Π_h a projection of $[L^2(\Omega)]^m$ into a finite element test space $\mathcal{M}^h$ contained in $[L^2(\Omega)]^m$. Furthermore, to $\mathcal{U}^h$ there corresponds a discrete space on the boundary, and we suppose for simplicity that the trace of $\boldsymbol{g}$ is an element of this space.

We assume that the scheme can be formulated as a discrete boundary value problem of the following type: find $\boldsymbol{u}_h \in \mathcal{U}^h$ such that

$$\Pi_h L\boldsymbol{u}_h = \Pi_h \boldsymbol{f} \ \text{ on } \Omega, \ \ B^-\boldsymbol{u}_h|_{\partial\Omega} = B^-\boldsymbol{g}|_{\partial\Omega}. \tag{3.27}$$

We suppose that this discrete problem has a unique solution.

Let $\boldsymbol{u} \in H(L,\Omega)$ be the exact weak/strong solution of the boundary value problem (2.2), (2.6). We denote by $\boldsymbol{e}_h := \boldsymbol{u} - \boldsymbol{u}_h$ the *global error* of the approximate solution and define the *residual*

$$\boldsymbol{r}_h = \boldsymbol{f} - L\boldsymbol{u}_h (= L\boldsymbol{e}_h) \ \in [L^2(\Omega)]^m.$$

In particular, we note that the global error $\boldsymbol{e}_h$ is the unique solution of the boundary value problem

$$L\boldsymbol{e}_h = \boldsymbol{r}_h \ \text{ on } \Omega, \ \ B^-\boldsymbol{e}_h|_{\partial\Omega} = 0.$$

Thus we have that $\boldsymbol{e}_h$ belongs to $D(L,\Omega)$. By taking $\boldsymbol{u} = \boldsymbol{e}_h$ in (3.23), we obtain the following error bounds for $\alpha = 0$.

Theorem 3.2 *Suppose that $\boldsymbol{u}_h \in \mathcal{U}^h \subset H(L,\Omega)$; then, we have the strong global a posteriori error bounds:*

$$\|\boldsymbol{r}_h\|_0 \le |||\boldsymbol{e}_h||| \le c_1\|\boldsymbol{r}_h\|_0. \tag{3.28}$$

Next we extend the process of a posteriori estimation to weaker norms. Noting that $\boldsymbol{e}_h \in D(L,\Omega)$ and using (2.14) and (3.26) we obtain, for $\alpha = 0$,

$$|||\boldsymbol{r}_h|||'_* = |||L\boldsymbol{e}_h|||'_* = \sup_{\boldsymbol{\phi}\in D(L^*,\Omega)} \frac{(L\boldsymbol{e}_h,\boldsymbol{\phi})}{|||\boldsymbol{\phi}|||_*} = \sup_{\boldsymbol{\phi}\in D(L^*,\Omega)} \frac{(\boldsymbol{e}_h,L^*\boldsymbol{\phi})}{|||\boldsymbol{\phi}|||_*}$$

$$\le \sup_{\boldsymbol{\phi}\in D(L^*,\Omega)} \frac{\|\boldsymbol{e}_h\|_0\|L^*\boldsymbol{\phi}\|_0}{|||\boldsymbol{\phi}|||_*} \le \|\boldsymbol{e}_h\|_0.$$

In the adjoint boundary value problem (3.25) we take $\boldsymbol{f} = \boldsymbol{e}_h$, $\boldsymbol{g} = \boldsymbol{0}$, and consider the corresponding (unique) solution $\boldsymbol{\varphi} \in D(L^*, \Omega)$. Now for $\boldsymbol{e}_h \in D(L, \Omega)$ we have, using (2.14) and (3.26), that

$$|||\boldsymbol{r}_h|||'_* = \sup_{\boldsymbol{\phi} \in D(L^*,\Omega)} \frac{(L\boldsymbol{e}_h, \boldsymbol{\phi})}{|||\boldsymbol{\phi}|||_*} \geq \frac{(L\boldsymbol{e}_h, \boldsymbol{\varphi})}{|||\boldsymbol{\varphi}|||_*} = \frac{(\,\boldsymbol{e}_h, L^*\boldsymbol{\varphi})}{|||\boldsymbol{\varphi}|||_*}$$

$$= \frac{(L^*\boldsymbol{\varphi}, L^*\boldsymbol{\varphi})}{|||\boldsymbol{\varphi}|||_*} = \frac{\|L^*\boldsymbol{\varphi}\|_0^2}{|||\boldsymbol{\varphi}|||_*} \geq \frac{1}{c_1}\|L^*\boldsymbol{\varphi}\|_0.$$

This proves the following global two-sided a posteriori error bound on the L^2 norm of the global error in terms of the dual (weighted) graph norm of the residual.

Theorem 3.3 *Assuming that $\alpha = 0$, we have the weak global a posteriori error bounds:*

$$|||\boldsymbol{r}_h|||'_* \leq ||\boldsymbol{e}_h||_0 \leq c_1|||\boldsymbol{r}_h|||'_*. \tag{3.29}$$

The next section is concerned with the decomposition of the error into a locally created part, called the *cell error*, and a propagating component which will be referred to as the *transmitted error*.

3.3. Cell error and transmitted error

Let $\kappa \subset \Omega$ be a cell in the partition of the domain. On κ we consider the exact solutions $\tilde{\boldsymbol{u}}$, $\tilde{\boldsymbol{u}}_h \in H(L, \Omega)$ of the local boundary value problems

$$L\tilde{\boldsymbol{u}} = \boldsymbol{f} \ \text{ on } \kappa, \quad B^-\tilde{\boldsymbol{u}}|_{\partial\kappa} = B^-\boldsymbol{u}|_{\partial\kappa}, \tag{3.30}$$

$$L\tilde{\boldsymbol{u}}_h = \boldsymbol{f} \ \text{ on } \kappa, \quad B^-\tilde{\boldsymbol{u}}_h|_{\partial\kappa} = B^-\boldsymbol{u}_h|_{\partial\kappa}. \tag{3.31}$$

Due to the unique solvability of the boundary value problem, we have that $\tilde{\boldsymbol{u}} = \boldsymbol{u}|_\kappa$.

For $\tilde{\boldsymbol{u}}_h$ we provide the following interpretation. Suppose that we have determined the numerical solution on Ω. Then $B^-\boldsymbol{u}_h|_{\partial\kappa}$ can be thought of as distorted boundary data due to the numerical error outside of the cell κ. In the second problem (3.31) above we consider the exact solution subject to these distorted numerical data. Then the quantity

$$\boldsymbol{e}_\kappa^{\text{cell}} = (\tilde{\boldsymbol{u}}_h - \boldsymbol{u}_h)|_\kappa \in D(L, \kappa)$$

represents the error produced by the scheme on this cell; we call it the *cell error*. The complementary quantity

$$\boldsymbol{e}_\kappa^{\text{trans}} = (\boldsymbol{u} - \tilde{\boldsymbol{u}}_h)|_\kappa$$

reflects the component of the error which is created outside of the cell; we name this part of the error the *transmitted error*. Therefore, on each cell we have the following decomposition of the global error:

$$\boldsymbol{e}_h|_\kappa = (\boldsymbol{u} - \boldsymbol{u}_h)|_\kappa = \boldsymbol{e}_\kappa^{\mathrm{cell}} + \boldsymbol{e}_\kappa^{\mathrm{trans}}.$$

The relevance of the cell error $\boldsymbol{e}_\kappa^{\mathrm{cell}}$ is that it is the part of the global error which directly contributes to the cell residual that we shall use as an error indicator. We deduce that the transmitted error satisfies

$$\begin{aligned} L\boldsymbol{e}_\kappa^{\mathrm{trans}} &= L\boldsymbol{u} - L\tilde{\boldsymbol{u}}_h = \mathbf{0} \quad \text{on } \kappa, \\ B^- \boldsymbol{e}_\kappa^{\mathrm{trans}}|_{\partial\kappa} &= B^-(\boldsymbol{u} - \boldsymbol{u}_h)|_{\partial\kappa} = B^- \boldsymbol{e}|_{\partial\kappa}. \end{aligned} \tag{3.32}$$

On the other hand, the cell error satisfies

$$\begin{aligned} \boldsymbol{r}_h = L\boldsymbol{e}_h = L\boldsymbol{e}_\kappa^{\mathrm{trans}} + L\boldsymbol{e}_\kappa^{\mathrm{cell}} = L\boldsymbol{e}_\kappa^{\mathrm{cell}} \quad \text{on } \kappa \\ B^- \boldsymbol{e}_\kappa^{\mathrm{cell}}|_{\partial\kappa} = \mathbf{0}. \end{aligned} \tag{3.33}$$

This shows that the cell residual $\boldsymbol{r}_h|_\kappa$ is only influenced by the cell error on the cell κ. Therefore, it is reasonable to attempt to improve the numerical solution by an adaptive procedure on those cells where the cell residual is largest. The next subsection focuses on the question of local error control: we derive local two-sided a posteriori error bounds on the cell error $\boldsymbol{e}_\kappa^{\mathrm{cell}}$ in terms of the (computable) local residual $\boldsymbol{r}_h|_\kappa$ in various norms.

3.4. Local a posteriori error estimates

Suppose that κ is a Lipschitz subdomain of Ω with a boundary $\partial\kappa$ that is almost everywhere non-characteristic for the operator L. In order to sharpen the global estimates, we shall assume that condition (2) in the definition of a symmetric positive system holds on each subdomain $\kappa \subset \Omega$ with a local constant $c_0 = c_0(\kappa)$. All of the results derived above on Ω also hold on the subset κ. In particular, since $\boldsymbol{e}_\kappa^{\mathrm{cell}}$ is the unique solution to the initial value problem

$$L\boldsymbol{e}_\kappa^{\mathrm{cell}} = \boldsymbol{r}_h \text{ on } \kappa, \quad B^- \boldsymbol{e}_\kappa^{\mathrm{cell}}|_{\partial\kappa} = 0,$$

we have that $\boldsymbol{e}_\kappa^{\mathrm{cell}}$ belongs to $D(L, \kappa)$. By taking $\boldsymbol{u} = \boldsymbol{e}_\kappa^{\mathrm{cell}} \mathrm{e}^{-\alpha(\xi \cdot x)}$ in (3.23) and repeating the reasoning presented in the previous section, we obtain the following error estimate.

Theorem 3.4 *Suppose that $\boldsymbol{u}_h \in \mathcal{U}^h \subset H(L,\Omega)$; then, we have the strong local a posteriori error bounds*

$$\min_{x\in\kappa} w(x)\|\boldsymbol{r}_h\|_{0,\kappa} \leq |||\boldsymbol{e}_\kappa^{\mathrm{cell}}|||_\kappa \leq c_1(\kappa) \max_{x\in\kappa} w(x)\|\boldsymbol{r}_h\|_{0,\kappa}, \tag{3.34}$$

where $w(x) = e^{-\alpha(\xi\cdot x)}$ and $c_1(\kappa) = (1 + 1/c_0(\kappa)^2)^{1/2}$.

In contrast with the two-sided bound on the cell-error, we only have an upper bound on the transmitted error $\boldsymbol{e}_\kappa^{\mathrm{trans}}$. This estimate is reminiscent of stability estimates used in the analysis of error transport in the context of ordinary differential equations.

Theorem 3.5 *Assuming that $\boldsymbol{e}_\kappa^{\mathrm{trans}} \in [H^1(\kappa)]^m$, the following bound holds:*

$$\begin{aligned} 2c_0(\kappa)\|w\boldsymbol{e}_\kappa^{\mathrm{trans}}\|_{0,\kappa}^2 + (B^+ w\boldsymbol{e}_\kappa^{\mathrm{trans}}, w\boldsymbol{e}_\kappa^{\mathrm{trans}})_{\partial\kappa} \\ \leq (-B^- w\boldsymbol{e}_\kappa^{\mathrm{trans}}, w\boldsymbol{e}_\kappa^{\mathrm{trans}})_{\partial\kappa}, \end{aligned}$$

where $w(x) = e^{-\alpha(\xi\cdot x)}$.

Proof. By considering $b[\boldsymbol{e}_\kappa^{\mathrm{trans}}, w^2\boldsymbol{e}_\kappa^{\mathrm{trans}}]$, proceeding analogously as in (3.19) and exploiting the fact that $L\boldsymbol{e}_\kappa^{\mathrm{trans}} = 0$ and hence $b[\boldsymbol{e}_\kappa^{\mathrm{trans}}, w^2\boldsymbol{e}_\kappa^{\mathrm{trans}}] = 0$, we obtain the desired inequality. □

Since B^+ and $-B^-$ are assumed to be positive definite, this estimate puts an upper bound on the transmitted error on κ and the outflow of transmitted error in terms of the incoming error.

Remark 3.6 In the case of a scalar hyperbolic equation, corresponding to $m = 1$, the following *non-local* upper bound on the transmitted error $\boldsymbol{e}_\kappa^{\mathrm{trans}}$ may be derived:

$$\|\boldsymbol{e}_\kappa^{\mathrm{trans}}\|_{\left(H_0^1(\kappa)\right)'} \leq C\|h\boldsymbol{r}_h\|_{L^2(D_h(\kappa))},$$

where C is a computable constant and $D_h(\kappa)$ denotes the union of all elements in the partition which intersect the domain of dependence of κ, cf. [30]. The proof of this a posteriori error bound is based on a hyperbolic duality argument using the general theoretical framework outlined in [31].

Now we consider the derivation of weak a posteriori bounds. For this purpose we consider $\boldsymbol{e}_\kappa^{\mathrm{cell}} \in D(L,\kappa)$ and use the weighted analogues of (2.14) and (3.26) to obtain

$$\begin{aligned} |||\boldsymbol{r}_h|||'_{*,\kappa} &= |||L\boldsymbol{e}_\kappa^{\mathrm{cell}}|||'_{*,\kappa} \\ &= \sup_{\boldsymbol{\phi}\in D(L^*,\kappa)} \frac{(L\boldsymbol{e}_\kappa^{\mathrm{cell}}, \boldsymbol{\phi})_\kappa}{|||\boldsymbol{\phi}|||_{*,\kappa}} \end{aligned}$$

$$
\begin{aligned}
&= \sup_{\boldsymbol{\phi}\in D(L^*,\kappa)} \frac{(\boldsymbol{e}_\kappa^{\mathrm{cell}}, L^*\boldsymbol{\phi})_\kappa}{|||\boldsymbol{\phi}|||_{*,\kappa}} \\
&\le \sup_{\boldsymbol{\phi}\in D(L^*,\kappa)} \frac{\|\mathrm{e}^{\alpha(\xi\cdot x)}\boldsymbol{e}_\kappa^{\mathrm{cell}}\|_{0,\kappa}\|\mathrm{e}^{-\alpha(\xi\cdot x)}L^*\boldsymbol{\phi}\|_{0,\kappa}}{|||\boldsymbol{\phi}|||_{*,\kappa}} \\
&\le \|\mathrm{e}^{\alpha(\xi\cdot x)}\boldsymbol{e}_\kappa^{\mathrm{cell}}\|_{0,\kappa} \\
&\le \max_{x\in\kappa}\hat{w}(x)\|\boldsymbol{e}_\kappa^{\mathrm{cell}}\|_{0,\kappa},
\end{aligned}
$$

where $\hat{w}(x) = \mathrm{e}^{\alpha(\xi\cdot x)}$. For the reverse inequality we consider on $\Omega = \kappa$ the adjoint boundary value problem (3.25) with $\boldsymbol{f} = \mathrm{e}^{-2\alpha(\xi\cdot x)}\boldsymbol{e}_\kappa^{\mathrm{cell}}$, $\boldsymbol{g} = \boldsymbol{0}$, and consider the corresponding (unique) solution $\boldsymbol{\varphi} \in D(L^*,\kappa)$. Now for $\boldsymbol{e}_\kappa^{\mathrm{cell}} \in D(L,\kappa)$ we have, using (2.14) and (3.26), that

$$
\begin{aligned}
|||\boldsymbol{r}_h|||'_{*,\kappa} &= \sup_{\boldsymbol{\phi}\in D(L^*,\kappa)} \frac{(L\boldsymbol{e}_\kappa^{\mathrm{cell}}, \boldsymbol{\phi})_\kappa}{|||\boldsymbol{\phi}|||_{*,\kappa}} \ge \frac{(L\boldsymbol{e}_\kappa^{\mathrm{cell}}, \boldsymbol{\varphi})_\kappa}{|||\boldsymbol{\varphi}|||_{*,\kappa}} = \frac{(\,\boldsymbol{e}_\kappa^{\mathrm{cell}}, L^*\boldsymbol{\varphi})_\kappa}{|||\boldsymbol{\varphi}|||_{*,\kappa}} \\
&= \frac{(\mathrm{e}^{\alpha(\xi\cdot x)}L^*\boldsymbol{\varphi}, \mathrm{e}^{\alpha(\xi\cdot x)}L^*\boldsymbol{\varphi})_\kappa}{|||\boldsymbol{\varphi}|||_{*,\kappa}} = \frac{\|\mathrm{e}^{\alpha(\xi\cdot x)}L^*\boldsymbol{\varphi}\|_{0,\kappa}^2}{|||\boldsymbol{\varphi}|||_{*,\kappa}} \\
&\ge \frac{1}{c_1(\kappa)}\|\mathrm{e}^{\alpha(\xi\cdot x)}L^*\boldsymbol{\varphi}\|_{0,\kappa} = \frac{1}{c_1(\kappa)}\|\mathrm{e}^{-\alpha(\xi\cdot x)}\boldsymbol{e}_\kappa^{\mathrm{cell}}\|_0.
\end{aligned}
$$

This proves the following local two-sided a posteriori error bound on the L^2 norm of the cell error in terms of the weighted dual graph norm of the residual.

Theorem 3.7 *We have the following local a posteriori error bounds:*

$$
\begin{aligned}
\min_{x\in\kappa} w(x)\,|||\boldsymbol{r}_h|||'_{*,\kappa} &\le ||\boldsymbol{e}_\kappa^{\mathrm{cell}}||_{0,\kappa} \\
&\le c_1(\kappa)\max_{x\in\kappa}[w(x)]^{-1}|||\boldsymbol{r}_h|||'_{*,\kappa}.
\end{aligned} \tag{3.35}
$$

The results of Theorems 3.4 and 3.7 also allow global error estimates to be derived. For example

$$
\begin{aligned}
|||\boldsymbol{e}^{\mathrm{cell}}||| &= \left\{\sum_\kappa |||\boldsymbol{e}_\kappa^{\mathrm{cell}}|||_\kappa^2\right\}^{\frac{1}{2}} \\
&\le \left\{\sum_\kappa (c_1(\kappa)\max_{x\in\kappa} w(x)||\boldsymbol{r}_h||_{0,\kappa})^2\right\}^{\frac{1}{2}} \\
&= \left\{\sum_\kappa (\bar{\epsilon}_1(\kappa))^2\right\}^{\frac{1}{2}} \equiv \bar{\epsilon}_1.
\end{aligned}
$$

Therefore, $\bar{\epsilon}_1(\kappa) = c_1(\kappa) \max_{x\in\kappa} w(x)||\boldsymbol{r}_h||_{0,\kappa}$ is a local upper estimator and $\bar{\epsilon}_1$ is a global upper estimate for $|||\boldsymbol{e}^{\rm cell}|||$. We also have

$$
\begin{aligned}
||\boldsymbol{e}^{\rm cell}||_0 &= \left\{ \sum_\kappa ||\boldsymbol{e}_\kappa^{\rm cell}||_{0,\kappa}^2 \right\}^{\frac{1}{2}} \\
&\leq \left\{ \sum_\kappa (c_1(\kappa) \max_{x\in\kappa} [w(x)]^{-1} |||\boldsymbol{r}_h|||'_{*,\kappa})^2 \right\}^{\frac{1}{2}} \\
&= \left\{ \sum_\kappa (\bar{\epsilon}_2(\kappa))^2 \right\}^{\frac{1}{2}} \equiv \bar{\epsilon}_2.
\end{aligned}
$$

Therefore, $\bar{\epsilon}_2(\kappa) = c_1(\kappa) \max_{x\in\kappa} [w(x)]^{-1} |||\boldsymbol{r}_h|||'_{*,\kappa}$ is a local upper estimator and $\bar{\epsilon}_2$ is a global upper estimate for $||\boldsymbol{e}^{\rm cell}||_0$.

We conclude this section by noting that estimates identical to the ones derived above hold for Friedrichs systems in conservation form.

4. Further bounds on the dual graph norm

The error estimates (3.34) and (3.35) derived in the previous section put sharp bounds on the locally created component of the global error in terms of the L^2 norm and the dual graph norm of the residual $\boldsymbol{r}_h$, respectively; unfortunately, the dual graph norm of $\boldsymbol{r}_h$ is difficult to compute (although in [24] it was approximated by partitioning the cell κ, and was successfully implemented into an adaptive finite volume algorithm for the numerical solution of the Euler equations of compressible gas dynamics). In this section we shall prove that $|||\boldsymbol{r}_h|||'_{*,\kappa}$ can be further bounded from above by a constant multiple of $\|h\boldsymbol{r}_h\|_{0,\kappa}$, a quantity that is simple and cheap to compute; we shall also prove that there is a similar lower bound. These bounds on the dual graph norm extend the results of [29] to Friedrichs systems in non-conservative form.

In the remainder of this section we shall assume that (2') holds instead of (2).

Theorem 4.1 *The following one-sided a posteriori error bound on the cell error in terms of the residual $\boldsymbol{r}_h$ is valid:*

$$\|\boldsymbol{e}_\kappa^{\rm cell}\|_{0,\kappa} \leq c_3(\kappa) \|h\boldsymbol{r}_h\|_{0,\kappa},$$

where

$$
\begin{aligned}
c_3(\kappa) &= c_2(\kappa)(1 + 1/c_0(\kappa)^2)^{1/2} \exp(\alpha(1+h)|\xi|), \\
c_2(\kappa) &= (h^2 + c_0'(\kappa)^2/4)^{-1/2} \exp(\alpha|\xi|),
\end{aligned}
$$

$c_0(\kappa)$ and $c_0'(\kappa)$ are the constants from conditions (2) and (2'), respectively, applied on the cell κ, and h denotes the diameter of κ.

Proof. Assume that ζ is in $\mathbb{R}^n$ (to be fixed later on) and let κ be any element in the partition of Ω. In order to simplify the argument we shall suppose that the origin of the coordinate system is the centroid of the element κ; if this is not the case then the exponential weight-function $\exp(\alpha(\zeta \cdot x))$ in the expressions below should be replaced by $\exp(\alpha(\zeta \cdot (x - x_c)))$ where x_c is the centroid of κ, the important property being that the weight function remains bounded on κ as $h = \operatorname{diam}(\kappa)$ converges to zero. Now for any ϕ in $D(L^*, \kappa)$ we have the following identity:

$$
\begin{aligned}
&-\int_\kappa \mathrm{e}^{2\alpha(\zeta\cdot x)} \left(\sum_{i=1}^n \frac{\partial}{\partial x_i}(A_i\phi) \right) \cdot \phi \, dx \\
&= -\int_{\partial\kappa} \mathrm{e}^{2\alpha(\zeta\cdot x)} \phi \cdot (B\phi)\, ds + 2\alpha \sum_{i=1}^n \int_\kappa \mathrm{e}^{2\alpha(\zeta\cdot x)} \phi \cdot (\zeta_i A_i \phi)\, dx \\
&\quad - \sum_{i=1}^n \int_\kappa \mathrm{e}^{2\alpha(\zeta\cdot x)} \phi \cdot \left(\frac{\partial A_i}{\partial x_i}\phi \right) dx \\
&\quad + \sum_{i=1}^n \int_\kappa \mathrm{e}^{2\alpha(\zeta\cdot x)} \phi \cdot \left(\frac{\partial}{\partial x_i}(A_i\phi) \right) dx.
\end{aligned}
$$

Transferring the last term on the right-hand side to the left, we obtain

$$
\begin{aligned}
&-\int_\kappa \mathrm{e}^{2\alpha(\zeta\cdot x)} \left(\sum_{i=1}^n \frac{\partial}{\partial x_i}(A_i\phi) \right) \cdot \phi \, dx \\
&= -\frac{1}{2} \int_{\partial\kappa} \mathrm{e}^{2\alpha(\zeta\cdot x)} \phi \cdot (B\phi)\, ds \\
&\quad + \int_\kappa \mathrm{e}^{2\alpha(\zeta\cdot x)} \phi \cdot \left(\alpha \sum_{i=1}^n \zeta_i A_i - \frac{1}{2} \sum_{i=1}^n \frac{\partial A_i}{\partial x_i} \right) \phi \, dx.
\end{aligned}
$$

Thus,

$$
\begin{aligned}
&\int_\kappa \mathrm{e}^{2\alpha(\zeta\cdot x)} \left(-\sum_{i=1}^n \frac{\partial}{\partial x_i}(A_i\phi) + C^*\phi \right) \cdot \phi \, dx \\
&= -\frac{1}{2} \int_{\partial\kappa} \mathrm{e}^{2\alpha(\zeta\cdot x)} \phi \cdot (B\phi)\, ds \\
&\quad + \int_\kappa \mathrm{e}^{2\alpha(\zeta\cdot x)} \phi \cdot \left(C + \alpha \sum_{i=1}^n \zeta_i A_i - \frac{1}{2} \sum_{i=1}^n \frac{\partial A_i}{\partial x_i} \right) \phi \, dx. \qquad (4.36)
\end{aligned}
$$

Noting that

$$\int_\kappa \mathrm{e}^{2\alpha(\zeta\cdot x)}\phi\cdot(C\phi)\,dx = \int_\kappa \mathrm{e}^{2\alpha(\zeta\cdot x)}(C^*\phi)\cdot\phi\,dx$$
$$= \int_\kappa \mathrm{e}^{2\alpha(\zeta\cdot x)}\phi\cdot(C^*\phi)\,dx,$$

and applying this in the second term on the right-hand side of (4.36) gives

$$\int_\kappa \mathrm{e}^{2\alpha(\zeta\cdot x)}\left(-\sum_{i=1}^n \frac{\partial}{\partial x_i}(A_i\phi)+C^*\phi\right)\cdot\phi\,dx$$
$$= -\frac{1}{2}\int_{\partial\kappa}\mathrm{e}^{2\alpha(\zeta\cdot x)}\phi\cdot(B\phi)\,ds$$
$$+\int_\kappa \mathrm{e}^{2\alpha(\zeta\cdot x)}\phi\cdot\left(C^*+\alpha\sum_{i=1}^n\zeta_iA_i-\frac{1}{2}\sum_{i=1}^n\frac{\partial A_i}{\partial x_i}\right)\phi\,dx. \tag{4.37}$$

Summing the identities (4.36) and (4.37), and recalling that $B=B^+ + B^-$ with $B^+\phi = 0$ on $\partial\Omega$ and $-\phi\cdot(B^-\phi)\geq 0$ on $\partial\Omega$, we conclude that

$$\int_\kappa \mathrm{e}^{2\alpha(\zeta\cdot x)}L^*\phi\cdot\phi\,dx \geq \int_\kappa \mathrm{e}^{2\alpha(\zeta\cdot x)}\phi\cdot\frac{1}{2}(K_\zeta(x)+K_\zeta^*(x))\phi\,dx.$$

In order to proceed, let us consider

$$\frac{1}{2}(K_\zeta(x)+K_\zeta^*(x)) = \frac{1}{2}(C+C^*)-\frac{1}{2}\sum_{i=1}^n\frac{\partial A_i}{\partial x_i}+\alpha\sum_{i=1}^n\zeta_iA_i.$$

Choosing $\zeta_i = h^{-1}\xi_i$, $i=1,...,n$, where $h=\mathrm{diam}(\kappa)$, and recalling (2') we have that

$$\frac{1}{2}(K_\zeta(x)+K_\zeta^*(x))$$
$$= h^{-1}\left(\alpha\sum_{i=1}^n\xi_iA_i+h\left(\frac{1}{2}(C+C^*)-\frac{1}{2}\sum_{i=1}^n\frac{\partial A_i}{\partial x_i}\right)\right)$$
$$\geq h^{-1}\left(\alpha c_0'(\kappa)I+h\left(\frac{1}{2}(C+C^*)-\frac{1}{2}\sum_{i=1}^n\frac{\partial A_i}{\partial x_i}\right)\right).$$

Since, by hypothesis, the entries of C and $\partial A_i/\partial x_i$ belong to $C(\overline{\Omega})$, it follows that, for h sufficiently small and all $x\in\kappa$,

$$\frac{1}{2}(K_\zeta(x)+K_\zeta^*(x)) \geq \frac{\alpha c_0'(\kappa)}{2h}I.$$

Thus we arrive at the local Gårding inequality

$$\int_\kappa \mathrm{e}^{2\alpha(\zeta\cdot x)} L^*\phi\cdot\phi\,dx \geq \frac{\alpha c_0'(\kappa)}{2h}\int_\kappa \mathrm{e}^{2\alpha(\zeta\cdot x)}|\phi|^2\,dx.$$

Applying the Cauchy-Schwarz inequality to the left-hand side, it follows that

$$\left(\int_\kappa \mathrm{e}^{2\alpha(\zeta\cdot x)}|\phi|^2\,dx\right)^{\frac{1}{2}} \leq \frac{2h}{\alpha c_0'(\kappa)}\left(\int_\kappa \mathrm{e}^{2\alpha(\zeta\cdot x)}|L^*\phi|^2\,dx\right)^{\frac{1}{2}}. \tag{4.38}$$

To complete the proof, we shall apply (4.38) to show that the dual graph norm of $\boldsymbol{r}_h$ is bounded above by a constant multiple of $\|h\boldsymbol{r}_h\|_0$; indeed,

$$|||\boldsymbol{r}_h|||'_{*,\kappa,\zeta} := \sup_{\phi\in D(L^*,\kappa)} \frac{|(\boldsymbol{r}_h,\phi)_\kappa|}{(\|\mathrm{e}^{\alpha(\zeta\cdot x)}\phi\|^2_{0,\kappa}+\|\mathrm{e}^{\alpha(\zeta\cdot x)}L^*\phi\|^2_{0,\kappa})^{\frac{1}{2}}}$$

$$\leq \sup_{\phi\in D(L^*,\kappa)} \frac{\|\mathrm{e}^{-\alpha(\zeta\cdot x)}\boldsymbol{r}_h\|_{0,\kappa}\|\mathrm{e}^{\alpha(\zeta\cdot x)}\boldsymbol{\phi}\|_{0,\kappa}}{(\|\mathrm{e}^{\alpha(\zeta\cdot x)}\phi\|^2_{0,\kappa}+\|\mathrm{e}^{\alpha(\zeta\cdot x)}L^*\phi\|^2_{0,\kappa})^{\frac{1}{2}}}$$

$$\leq h(h^2+\alpha^2 c_0'(\kappa)^2/4)^{-1/2}\|\mathrm{e}^{-\alpha(\zeta\cdot x)}\boldsymbol{r}_h\|_{0,\kappa}.$$

However, $|\alpha(\zeta\cdot x)| = h^{-1}\alpha|\xi\cdot x|$ with $h(<1)$ denoting the diameter of κ, so that, recalling that the origin of the coordinate system has been placed at the centroid of κ and therefore $|x|\leq h$ for x in κ, it follows that $|\alpha(\zeta\cdot x)|\leq\alpha|\xi|$ for $x\in\kappa$. Hence,

$$|||\boldsymbol{r}_h|||'_{*,\kappa,\zeta} \leq c_2(\kappa)\|h\boldsymbol{r}_h\|_{0,\kappa},$$

where $c_2(\kappa) = \mathrm{e}^{\alpha|\xi|}(h^2+\alpha^2c_0'(\kappa)^2/4)^{-1/2}$. Noting that

$$|||\phi|||_{*,\kappa} \equiv |||\phi|||_{*,\kappa,\xi} := (\|\mathrm{e}^{\alpha(\xi\cdot x)}\phi\|^2_{0,\kappa}+\|\mathrm{e}^{\alpha(\xi\cdot x)}L^*\phi\|^2_{0,\kappa})^{\frac{1}{2}}$$

and writing

$$\mathrm{e}^{\alpha(\xi\cdot x)} = \mathrm{e}^{\alpha(\zeta\cdot x)}\mathrm{e}^{-\alpha(\zeta-\xi)\cdot x} = \mathrm{e}^{\alpha(\zeta\cdot x)}\mathrm{e}^{-\alpha\xi(1-h)\cdot(x/h)},$$

we have that

$$\mathrm{e}^{-\alpha|\xi|}|||\phi|||_{*,\kappa,\zeta} \leq |||\phi|||_{*,\kappa,\xi}.$$

Thus,

$$|||\boldsymbol{r}_h|||'_{*,\kappa,\xi} = \sup_{\phi\in D(L^*,\kappa)}\frac{|(\boldsymbol{r}_h,\phi)_\kappa|}{|||\phi|||_{*,\kappa,\xi}} \leq \mathrm{e}^{\alpha|\xi|}|||\boldsymbol{r}_h|||'_{*,\kappa,\zeta}.$$

Now (3.35) states that,

$$\|\boldsymbol{e}_\kappa^{\rm cell}\|_{0,\kappa} \leq c_1(\kappa) \max_{x\in\kappa} \mathrm{e}^{\alpha(\xi\cdot x)} |||\boldsymbol{r}_h|||'_{*,\kappa,\xi},$$

and therefore

$$\begin{aligned}\|\boldsymbol{e}_\kappa^{\rm cell}\|_{0,\kappa} &\leq c_1(\kappa)\mathrm{e}^{\alpha h|\xi|}\mathrm{e}^{\alpha|\xi|}|||\boldsymbol{r}_h|||'_{*,\kappa,\zeta} \\ &\leq c_1(\kappa)c_2(\kappa)\mathrm{e}^{\alpha(1+h)|\xi|}\|h\boldsymbol{r}_h\|_{0,\kappa}.\end{aligned}$$

Hence, defining $c_3(\kappa) = c_1(\kappa)c_2(\kappa)\mathrm{e}^{\alpha(1+h)|\xi|}$, we obtain the desired bound

$$\|\boldsymbol{e}_\kappa^{\rm cell}\|_{0,\kappa} \leq c_3(\kappa)\|h\boldsymbol{r}_h\|_{0,\kappa}. \qquad \square$$

Now we prove an analogous lower bound; to do so, we consider a uniformly regular micro-partition of the cell κ, and let $S^{h_0} = S^{h_0}(\kappa)$ be a finite element subspace of $D(L^*,\kappa)$ on this micro-partition, with $h_0 = h_0(\kappa)$ denoting the maximum diameter of elements in the micro-partition. We denote by P_{h_0} the orthogonal projector in $[L^2(\kappa)]^m$ onto the finite element space S^{h_0}.

Theorem 4.2 *The following a posteriori lower bound on the cell error is valid:*

$$c_4(\kappa)\|h_0 P_{h_0}\boldsymbol{r}_h\|_{0,\kappa} \leq \|\boldsymbol{e}_\kappa^{\rm cell}\|_{0,\kappa},$$

where $c_4(\kappa)$ is a computable constant.

Proof. Since $S^{h_0} = S^{h_0}(\kappa)$ is contained in $D(L^*,\kappa)$, it follows that

$$\begin{aligned}|||\boldsymbol{r}_h|||'_{*,\kappa,\xi} &= \sup_{\phi\in D(L^*,\kappa)} \frac{|(\boldsymbol{r}_h,\phi)_\kappa|}{(\|\mathrm{e}^{\alpha(\xi\cdot x)}\phi\|_{0,\kappa}^2 + \|\mathrm{e}^{\alpha(\xi\cdot x)}L^*\phi\|_{0,\kappa}^2)^{\frac{1}{2}}} \\ &\geq \sup_{\phi_{h_0}\in S^{h_0}} \frac{|(\boldsymbol{r}_h,\phi_{h_0})_\kappa|}{(\|\mathrm{e}^{\alpha(\xi\cdot x)}\phi_{h_0}\|_{0,\kappa}^2 + \|\mathrm{e}^{\alpha(\xi\cdot x)}L^*\phi_{h_0}\|_{0,\kappa}^2)^{\frac{1}{2}}}. \qquad (4.39)\end{aligned}$$

Exploiting a standard inverse inequality in S^{h_0}, we deduce that

$$\left(\sum_{i=1}^n \|\mathrm{e}^{\alpha(\xi\cdot x)}\frac{\partial\phi_{h_0}}{\partial x_i}\|_{0,\kappa}^2\right)^{\frac{1}{2}} \leq \frac{c_5(\kappa)}{h_0}\|\mathrm{e}^{\alpha(\xi\cdot x)}\phi_{h_0}\|_{0,\kappa}, \qquad \phi_{h_0}\in S^{h_0},$$

and therefore, for all $\phi_{h_0}\in S^{h_0}$,

$$\begin{aligned}&\|\mathrm{e}^{\alpha(\xi\cdot x)}L^*\phi_{h_0}\|_{0,\kappa} \\ &\leq \sum_{i=1}^n \|A_i\|_{L_\infty(\kappa)}\|\mathrm{e}^{\alpha(\xi\cdot x)}\frac{\partial\phi_{h_0}}{\partial x_i}\|_{0,\kappa} + \|D\|_{L_\infty(\kappa)}\|\mathrm{e}^{\alpha(\xi\cdot x)}\phi_{h_0}\|_{0,\kappa}\end{aligned}$$

$$
\begin{aligned}
&\leq \left(\sum_{i=1}^{n} \|A_i\|^2_{L_\infty(\kappa)}\right)^{\frac{1}{2}} \left(\sum_{i=1}^{n} \|\mathrm{e}^{\alpha(\xi\cdot x)} \frac{\partial \phi_{h_0}}{\partial x_i}\|^2_{0,\kappa}\right)^{\frac{1}{2}} \\
&\quad + \|D\|_{L_\infty(\kappa)} \|\mathrm{e}^{\alpha(\xi\cdot x)} \phi_{h_0}\|_{0,\kappa} \\
&\leq \frac{1}{h_0} \left(h_0 \|D\|_{L_\infty(\kappa)} + c_5(\kappa) \left(\sum_{i=1}^{n} \|A_i\|^2_{L_\infty(\kappa)}\right)^{\frac{1}{2}} \right) \|\mathrm{e}^{\alpha(\xi\cdot x)} \phi_{h_0}\|_{0,\kappa} \\
&\equiv h_0^{-1} c_6(\kappa) \|\mathrm{e}^{\alpha(\xi\cdot x)} \phi_{h_0}\|_{0,\kappa},
\end{aligned}
$$

where $D = C^* - \sum_{i=1}^{n} \partial A_i / \partial x_i$. Substituting this bound into (4.39) gives

$$
\begin{aligned}
|||\boldsymbol{r}_h|||'_{*,\kappa,\xi} &\geq h_0 (h_0^2 + c_6(\kappa)^2)^{-1/2} \sup_{\phi_{h_0} \in S^{h_0}} \frac{|(\boldsymbol{r}_h, \phi_{h_0})_\kappa|}{\|\mathrm{e}^{\alpha(\xi\cdot x)} \phi_{h_0}\|_{0,\kappa}} \\
&\geq \frac{h_0 \mathrm{e}^{-\alpha h|\xi|}}{(h_0^2 + c_6(\kappa)^2)^{1/2}} \sup_{\phi_{h_0} \in S^{h_0}} \frac{|(P_{h_0} \boldsymbol{r}_h, \phi_{h_0})_\kappa|}{\|\phi_{h_0}\|_{0,\kappa}} \\
&= \mathrm{e}^{-\alpha h|\xi|} (h_0^2 + c_6(\kappa)^2)^{-\frac{1}{2}} \|h_0 P_{h_0} \boldsymbol{r}_h\|_{0,\kappa}.
\end{aligned}
$$

Combining this inequality with the lower bound on the cell error stated in Theorem 3.7 we arrive at the desired lower bound on $\|\boldsymbol{e}_\kappa^{\mathrm{cell}}\|_{0,\kappa}$. □

The bounds in Theorems 4.1 and 4.2 can be summarised as follows:

$$
c_4(\kappa) \|h_0 P_{h_0} \boldsymbol{r}_h\|_{0,\kappa} \leq \|\boldsymbol{e}_\kappa^{\mathrm{cell}}\|_{0,\kappa} \leq c_3(\kappa) \|h \boldsymbol{r}_h\|_{0,\kappa}, \tag{4.40}
$$

where $c_3(\kappa)$ and $c_4(\kappa)$ are computable constants. We note here that while the two-sided bound on the L^2 norm of the cell error given in Theorem 3.7 is sharp, inequality (4.40) is not, because of the mismatch between the expressions under the norm signs in the lower and the upper estimate. By virtue inequality of (4.40), we have the 'almost sharp' two-sided global estimate

$$
\begin{aligned}
\left(\sum_{\kappa} c_4(\kappa)^2 \|h_0 P_{h_0} \boldsymbol{r}_h\|^2_{0,\kappa}\right)^{\frac{1}{2}} &\leq \|\boldsymbol{e}^{\mathrm{cell}}\|_0 \\
&\leq \left(\sum_{\kappa} c_3(\kappa)^2 \|h \boldsymbol{r}_h\|^2_{0,\kappa}\right)^{\frac{1}{2}} \\
&\equiv \left\{\sum_{\kappa} (\overline{\epsilon}_3(\kappa))^2\right\}^{\frac{1}{2}} \equiv \overline{\epsilon}_3
\end{aligned}
$$

which now provides a global bound on the locally created component of the error.

5. Computational implementation and numerical experiments

In this section we assess the computational performance of the local a posteriori error bounds derived in this paper. We begin in Sect. 5.1 by discussing a practical approach to approximating the dual graph norm. Then, in Sect. 5.2 we describe an adaptive algorithm for automatically controlling the cell error with respect to a user-defined tolerance. Finally, in Sects. 5.3–5.6 we present a number of numerical experiments: Sects. 5.3–5.5 are devoted to the performance of $\bar{\epsilon}_1$ and $\bar{\epsilon}_2$ for the cell vertex scheme on uniform quadrilateral meshes. This cell vertex scheme is described in the papers [25–27, 3, 19], and can be formulated as a Petrov-Galerkin finite element method based on continuous piecewise bilinear trial functions and piecewise constant test functions. It is this latter interpretation that conforms with the framework described above. For cell centre finite volume methods, a similar construction is given in [28]. In Sect. 5.6 we illustrate the performance of the streamline-diffusion method on both uniform and adaptively refined triangular meshes using $\bar{\epsilon}_3$ as a local error indicator. We note that the streamline-diffusion method is based on a consistent perturbation of the standard Galerkin finite element method by adding a weighted least squares term to the standard test function $\boldsymbol{v}$: for the Friedrichs system (2.2), this corresponds to a test function of the form $\boldsymbol{v} + \delta L\boldsymbol{v}$, where $\delta = C_\delta h$, C_δ is a constant and h is a mesh function, cf. [12], for example.

In each of the numerical experiments presented, an approximation of the cell error and the transmitted error is obtained by numerically solving the local boundary value problems satisfied on each element κ by these quantities. The numerical solution to these local problems is computed using the underlying discretisation method (i.e. the cell vertex method in Examples 1–3 and the streamline-diffusion method in Example 4) on a mesh generated by four successive subdivisions of the element κ: for quadrilateral elements, this corresponds to a 17×17 subdivision of κ.

5.1. Estimating the dual graph norm

To evaluate the upper error estimate we need to calculate

$$|||\boldsymbol{r}_h|||'_{*,\kappa} = \sup_{\phi \in D(L^*,\kappa)} \frac{(\boldsymbol{r}_h, \phi)_\kappa}{|||\phi|||_{*,\kappa}}.$$

In practice, it is impossible to test the residual against every element in $D(L^*, \kappa)$. A computable approximation of $|||\boldsymbol{r}_h|||'_{*,\kappa}$ is obtained by evaluating

$$\max_{\phi \in S^{h_0} \subset D(L^*,\kappa)} \frac{(\boldsymbol{r}_h, \phi)_\kappa}{|||\phi|||_{*,\kappa}},$$

where S^{h_0} is a finite element subspace of $D(L^*, \kappa)$ on a micropartition of κ of granularity h_0. In the examples that follow, we use the following approximation for quadrilateral elements

$$|||\boldsymbol{r}_h|||'_{*,\kappa} \approx \max_{l,m=1,\ldots,NL} \frac{(\boldsymbol{r}_h, \phi_{lm})_\kappa}{|||\phi_{lm}|||_{*,\kappa}},$$

where each $\phi_{lm} \in D(L^*, \kappa)$ is a bilinear function on κ. For example, if we are interested in a two-dimensional scalar advection problem with convective velocity field $\boldsymbol{a} = (a_1, a_2)$, $a_i > 0$, $i = 1, 2$, then on each κ

$$\phi_{lm}(x_1, x_2) = \hat{\phi}_l(\hat{x}_1)\hat{\phi}_m(\hat{x}_2) \circ F_\kappa^{-1}$$

where F_κ is the mapping from local to global coordinates,

$$\phi_l(\hat{x}_1) = (\hat{x}_1 - 1)/((\hat{x}_1)_l - 1), \quad (\hat{x}_1)_l = \frac{2(l-1)}{NL} - 1,$$
$$l = 1, \ldots, NL,$$

and

$$\phi_m(\hat{x}_2) = (\hat{x}_2 - 1)/((\hat{x}_2)_m - 1), \quad (\hat{x}_2)_m = \frac{2(m-1)}{NL} - 1,$$
$$m = 1, \ldots, NL.$$

Each bilinear function is therefore zero on the outflow boundary of κ and is equal to unity at the image of $((\hat{x}_1)_l, (\hat{x}_2)_m)$. Numerical experience suggests that NL need not be large, and in the experiments below $NL = 3$. For further details concerning the approximate computation of the dual graph norm we refer to the paper of Sonar [23].

5.2. Adaptive algorithm

For a given tolerance TOL, we consider the problem of constructing a mesh such that:

$$\|\boldsymbol{e}^{\text{cell}}\|_0 \leq \text{TOL} \tag{5.41}$$

and the number of degrees of freedom is minimal. In order to satisfy the first condition, we exploit the a posteriori error estimate derived in Theorem 4.1; i.e. if we impose that

$$\overline{\epsilon}_3(\kappa) \leq \frac{\text{TOL}}{\sqrt{N}} \tag{5.42}$$

for each element κ in our mesh $\mathcal{T}$, where N is the number of elements in $\mathcal{T}$, then (5.41) will be automatically satisfied. For efficiency we try to ensure that (5.42) is satisfied with near equality, cf. [31].

In order to generate a mesh which will satisfy (5.42) for all κ in $\mathcal{T}$, subject to the efficiency constraint, we must employ a mesh modification strategy. In this paper we combine the use of a mesh subdivision algorithm (h-refinement) with a mesh movement algorithm (r-refinement). The subdivision algorithm is based on the well-known red-green isotropic refinement strategy, cf. [4]. Here, a red refinement corresponds to dividing a triangle into four similar triangles by connecting the midpoints of the sides. Green refinement is only temporary and is used to eliminate any hanging nodes created by a red refinement. We note that green refinement is only used on elements with one hanging node; elements with two or more hanging nodes are red refined.

The r-refinement algorithm is based on the very simple mesh movement strategy described in [8]. Here, the nodes are moved to a weighted average of the positions of the centroids of the neighbouring triangles. The new nodal position can thus be written as

$$x_n^{\text{new}} = \frac{\sum_{i=1}^{l_n} w_{\kappa_i} x_{\kappa_i}^{\text{c}}}{\sum_{i=1}^{l_n} w_{\kappa_i}}; \tag{5.43}$$

here $x_{\kappa_i}^{\text{c}}$ denotes the centroid of element κ_i and w_{κ_i} the element weight, where i runs over the elements adjacent to node n. Here, we define the element weight w_{κ_i} to be $\bar{\epsilon}_3(\kappa_i)$. To prevent mesh tangling, we limit the distance a node can move by imposing the following restriction

$$(\Delta x)_{\max} = \min_{i=1,\ldots,l_n} \left(\frac{\text{meas}(\kappa_i)}{h_{\kappa_i}} \right), \tag{5.44}$$

where $h_{\kappa_i} = \text{diam}(\kappa_i)$. A second restriction is also imposed to prevent the elements becoming too distorted.

For the implementation of this hr-refinement algorithm, we first specify an initial background mesh $\mathcal{T}_j$, $j = 1$, upon which we calculate a numerical approximation $\boldsymbol{u}_h$ to $\boldsymbol{u}$. Based on $\boldsymbol{u}_h$ we compute $\bar{\epsilon}_3$ and test to see if $\bar{\epsilon}_3$ is less than the prescribed tolerance TOL. If this is the case then the adaptive algorithm terminates; otherwise we modify the mesh as follows: if j is an odd number, then move the nodes of the mesh according to conditions (5.43) and (5.44). We note that for each j we loop over all the nodes in the mesh 20 times in order to generate the new mesh $\mathcal{T}_{j+1}$. If j is even, then subdivide the elements which fail to satisfy condition (5.42), and construct $\mathcal{T}_{j+1}$; we remark that elements may also be de-refined. Finally, we set $j = j + 1$, compute a numerical solution on the new mesh, and test the stopping criterion again. This process is repeated until the estimated cell error is below the given tolerance TOL.

Table 1. $||\boldsymbol{e}_h||_0$ and $||\boldsymbol{e}^{\mathrm{trans}}||_0$ for Example 1

Mesh	$\|\boldsymbol{e}_h\|_0$	k	$\|\boldsymbol{e}^{\mathrm{trans}}\|_0$	k
17×17	2.014×10^{-3}	-	2.050×10^{-2}	-
33×33	5.793×10^{-3}	1.80	5.945×10^{-3}	1.79
65×65	1.491×10^{-3}	1.96	1.534×10^{-3}	1.95
129×129	3.750×10^{-4}	1.99	3.860×10^{-4}	1.99
257×257	9.390×10^{-5}	2.00	9.662×10^{-5}	2.00

Table 2. $|||\boldsymbol{e}^{\mathrm{cell}}|||$ and $\bar{\epsilon}_1$ for Example 1

Mesh	$\|\|\|\boldsymbol{e}^{\mathrm{cell}}\|\|\|$	k	$\bar{\epsilon}_1$	k	θ_1
17×17	1.611×10^{-1}	-	3.188×10^{-1}	-	1.98
33×33	8.415×10^{-2}	0.94	1.650×10^{-1}	0.95	1.97
65×65	4.258×10^{-2}	0.98	8.330×10^{-2}	0.99	1.95
129×129	2.136×10^{-2}	1.00	4.174×10^{-2}	1.00	1.95
257×257	1.069×10^{-2}	1.00	2.089×10^{-2}	1.00	1.95

5.3. Example 1

The first example considered is a scalar advection problem of the form

$$\nabla.(\boldsymbol{a}u) = f, \qquad x \in (0,1)^2. \tag{5.45}$$

We take $f = 0$, $\boldsymbol{a} = (\cos(\pi/6), \sin(\pi/6))^{\mathrm{T}}$ and boundary conditions

$$u(x_1, 0) = \exp(-50x_1^4),$$
$$u(0, x_2) = 1.$$

To test the sharpness of the error estimates, calculations were performed on a sequence of uniform meshes. Table 1 shows $||\boldsymbol{e}_h||_0$ and $||\boldsymbol{e}^{\mathrm{trans}}||_0$ and their respective rates of convergence k. Since the exact solution is smooth, we observe second-order convergence. Figures 1(a) and (b) depict the distribution of the global and transmitted errors, respectively, on a 33×33 uniform mesh; the two errors are very similar and grow almost linearly from the inflow to the outflow boundary. The behaviour of $|||\boldsymbol{e}^{\mathrm{cell}}|||$ and its upper estimate $\bar{\epsilon}_1$ are shown in Table 2. Clearly, both quantities converge as $O(h)$. The final column of Table 2 shows the effectivity index $\theta_1 = \bar{\epsilon}_1/|||\boldsymbol{e}^{\mathrm{cell}}|||$, which indicates that $\bar{\epsilon}_1$ slightly overestimates $|||\boldsymbol{e}^{\mathrm{cell}}|||$. Figures 1(c) and (d) depict the distribution of $|||\boldsymbol{e}^{\mathrm{cell}}|||_\kappa$ and $\bar{\epsilon}_1(\kappa)$, respectively, which are in excellent agreement. The values of $||\boldsymbol{e}^{\mathrm{cell}}||_0$ and $\bar{\epsilon}_2$ are shown in Table 3, where the dual graph norm has been estimated as outlined in Sect. 5.1. We see that $||\boldsymbol{e}^{\mathrm{cell}}||_0$ and $\bar{\epsilon}_2$ both converge as $O(h^2)$ and that $\bar{\epsilon}_2$ slightly underestimates $||\boldsymbol{e}^{\mathrm{cell}}||_0$. Finally, Figs. 1(e) and (f) show that the distribution of $||\boldsymbol{e}^{\mathrm{cell}}||_0$ and $\bar{\epsilon}_2(\kappa)$, respectively, closely resemble each other. Plots of the distribution of $\bar{\epsilon}_3(\kappa)$ show a similar qualitative behaviour. Note that the distribution of

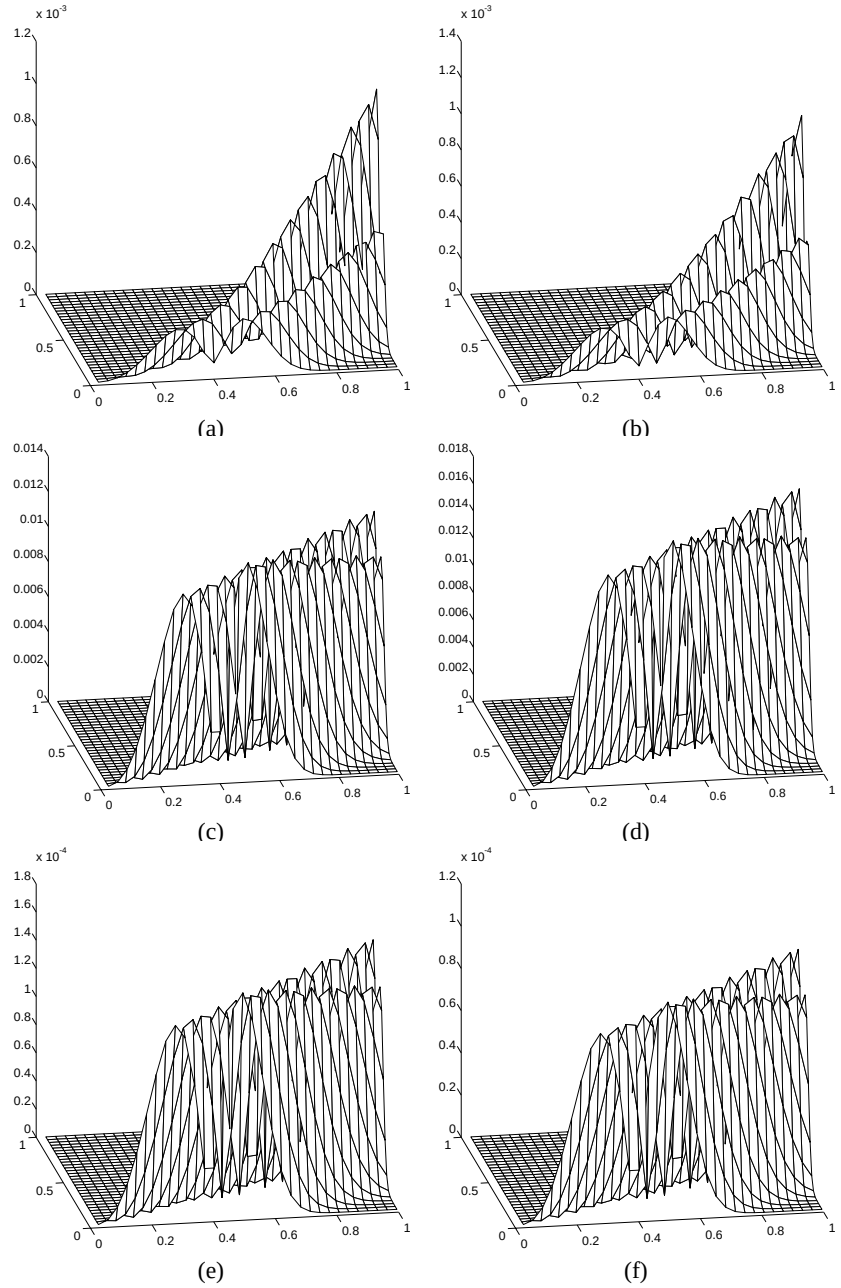

Fig. 1. Example 1: (a) $\|\boldsymbol{e}_h\|_{0,\kappa}$; (b) $\|\boldsymbol{e}^{\mathrm{trans}}\|_{0,\kappa}$; (c) $|||\boldsymbol{e}^{\mathrm{cell}}|||_{\kappa}$; (d) $\bar{\epsilon}_1(\kappa)$; (e) $||\boldsymbol{e}^{\mathrm{cell}}||_{0,\kappa}$; (f) $\bar{\epsilon}_2(\kappa)$

the cell error is quite different in character to the distribution of the global error. Although the cell error is largest along the line of steepest slope of the approximate solution, its value is almost constant, whereas the global error is linearly increasing. This suggests that a constant local error is being generated along characteristic paths from the inflow-boundary data.

5.4. Example 2

For the second example we consider the same scalar advection equation as in Example 1, with forcing function $f = 0$, advective velocity $\boldsymbol{a} = (\cos(\pi/6), \sin(\pi/6))^{\mathrm{T}}$ and boundary conditions

$$u(x_1, 0) = 0,$$
$$u(0, x_2) = 1.$$

For this problem with discontinuous solution, we expect the cell vertex finite volume approximation to converge to the analytical solution at the rate $O(h^{1/3})$, in accordance with the optimal error bounds presented in [3]. Table 4 shows that $||\boldsymbol{e}_h||_0$ and $||\boldsymbol{e}^{\mathrm{trans}}||_0$ converge at the same rate which is close to $1/3$. The two errors, which are depicted in Figs. 2(a) and (b), respectively, are largest along the line of discontinuity of the solution and, as with Example 1, grow linearly from the inflow to the outflow. Table 5 shows $|||\boldsymbol{e}^{\mathrm{cell}}|||$ and $\bar{\epsilon}_1$; as the exact solution to this problem is discontinuous, it is not surprising that the approximate solution does not converge in the graph norm. However, $\bar{\epsilon}_1$ faithfully remains an upper estimate and only slightly overestimates $|||\boldsymbol{e}^{\mathrm{cell}}|||_\kappa$. The distributions of $|||\boldsymbol{e}^{\mathrm{cell}}|||_\kappa$ and $\bar{\epsilon}_1(\kappa)$ are given in Figs. 2(c) and (d), respectively; we observe that the cell error is quite different in character to the global error. The cell error is largest at the introduction of the discontinuity into the domain and is then almost constant in a direction which is not along the line of discontinuity. A Fourier analysis of the cell vertex method shows that the error is entirely dispersive in nature and the cell error propagation is determined by the group velocity of the highest frequency component of the approximate solution [16]. Table 6 shows that $||\boldsymbol{e}^{\mathrm{cell}}||_0$ and $\bar{\epsilon}_2$ both converge as $O(h^{1/2})$, and that $\bar{\epsilon}_2(\kappa)$ slightly underestimates the error. Plots of the distribution of $||\boldsymbol{e}^{\mathrm{cell}}||_{0,\kappa}$ and $\bar{\epsilon}_2(\kappa)$ in Figs. 2(e) and (f), respectively, show that the local error estimate closely resembles the local cell error. Again, $||\boldsymbol{e}^{\mathrm{cell}}||_0$ is largest at the inflow of the domain and is distributed similarly to $|||\boldsymbol{e}^{\mathrm{cell}}|||$. To control the cell error, attention should be paid to the introduction of the discontinuity into the domain before any further calculations are performed.

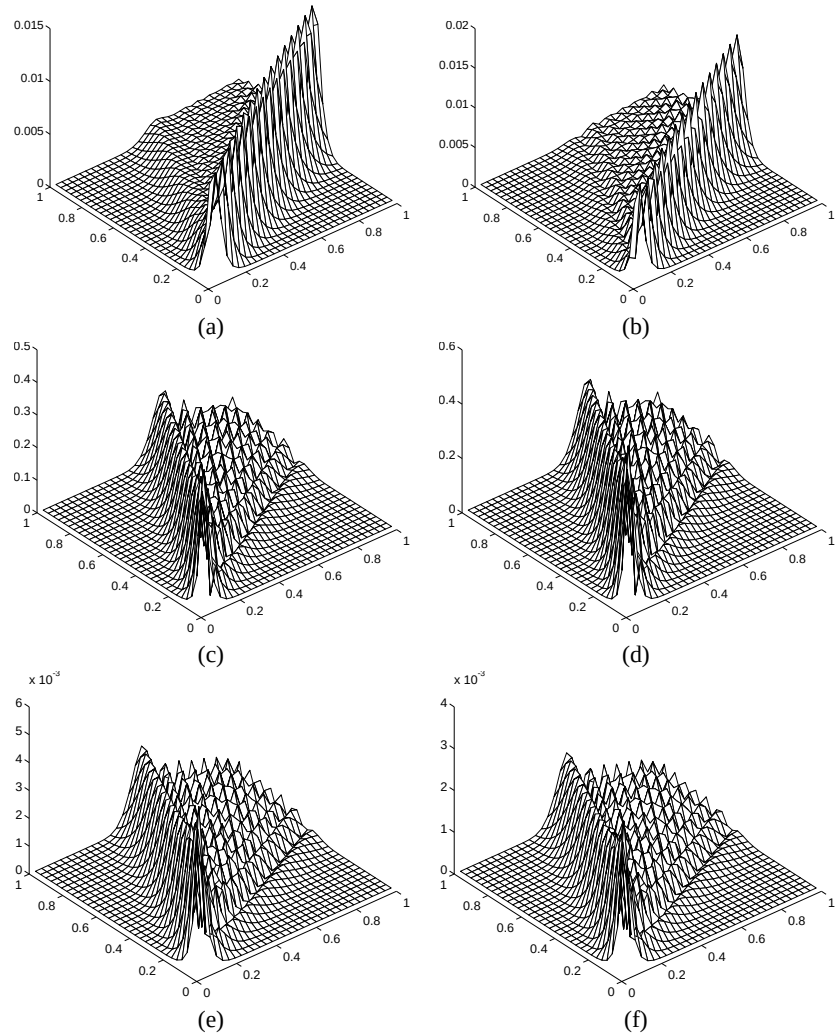

Fig. 2. Example 2: (a) $\|\boldsymbol{e}_h\|_{0,\kappa}$; (b) $\|\boldsymbol{e}^{\mathrm{trans}}\|_{0,\kappa}$; (c) $|||\boldsymbol{e}^{\mathrm{cell}}|||_{\kappa}$; (d) $\bar{\epsilon}_1(\kappa)$; (e) $||\boldsymbol{e}^{\mathrm{cell}}||_{0,\kappa}$; (f) $\bar{\epsilon}_2(\kappa)$

Table 3. $\|\boldsymbol{e}^{\mathrm{cell}}\|_0$ and $\bar{\epsilon}_2$ for Example 1

Mesh	$\|\boldsymbol{e}^{\mathrm{cell}}\|_0$	k	$\bar{\epsilon}_2$	k	θ_2
17×17	5.607×10^{-3}	-	5.248×10^{-3}	-	0.94
33×33	1.452×10^{-3}	1.95	1.360×10^{-3}	1.95	0.94
65×65	3.663×10^{-4}	1.99	3.430×10^{-4}	1.99	0.94
129×129	9.179×10^{-5}	2.00	8.595×10^{-5}	2.00	0.94
257×257	2.296×10^{-5}	2.00	2.150×10^{-5}	2.00	0.94

Table 4. $||e_h||_0$ and $||e^{\mathrm{trans}}||_0$ for Example 2

Mesh	$\|e_h\|_0$	k	$\|e^{\mathrm{trans}}\|_0$	k
17×17	1.333×10^{-1}	-	1.333×10^{-1}	-
33×33	1.105×10^{-1}	0.27	1.100×10^{-1}	0.27
65×65	9.104×10^{-2}	0.28	9.035×10^{-2}	0.27
129×129	7.447×10^{-2}	0.29	7.408×10^{-2}	0.28
257×257	6.055×10^{-2}	0.30	6.029×10^{-2}	0.29

Table 5. $|||e^{\mathrm{cell}}|||$ and $\bar{\epsilon}_1$ for Example 2

Mesh	$\|\|\|e^{\mathrm{cell}}\|\|\|$	k	$\bar{\epsilon}_1$	k	θ_1
17×17	2.708	-	3.830	-	1.41
33×33	3.834	-0.50	5.422	-0.50	1.41
65×65	5.425	-0.50	7.672	-0.50	1.41
129×129	7.675	-0.50	10.854	-0.50	1.41
257×257	10.855	-0.50	15.351	-0.50	1.41

Table 6. $\|e^{\mathrm{cell}}\|_0$ and $\bar{\epsilon}_2$ for Example 2

Mesh	$\|e^{\mathrm{cell}}\|_0$	k	$\bar{\epsilon}_2$	k	θ_2
17×17	4.963×10^{-2}	-	4.241×10^{-2}	-	0.85
33×33	3.514×10^{-2}	0.50	3.003×10^{-2}	0.50	0.85
65×65	2.486×10^{-2}	0.50	2.125×10^{-2}	0.50	0.85
129×129	1.758×10^{-2}	0.50	1.503×10^{-2}	0.50	0.85
257×257	1.243×10^{-2}	0.50	1.063×10^{-2}	0.50	0.85

5.5. Example 3

Here, we consider the cell vertex method applied to the one-dimensional wave equation

$$\frac{\partial^2 \phi}{\partial x_2^2} = c^2 \frac{\partial^2 \phi}{\partial x_1^2}, \tag{5.46}$$

which can be rewritten as the symmetric first-order system

$$\begin{bmatrix} 0 & -c \\ -c & 0 \end{bmatrix} \begin{bmatrix} u_1 \\ u_2 \end{bmatrix}_{x_1} + \begin{bmatrix} 1 & 0 \\ 0 & 1 \end{bmatrix} \begin{bmatrix} u_1 \\ u_2 \end{bmatrix}_{x_2} = \begin{bmatrix} 0 \\ 0 \end{bmatrix}, \tag{5.47}$$

where

$$u_1 = \frac{\partial \phi}{\partial x_2} \quad \text{and} \quad u_2 = c \frac{\partial \phi}{\partial x_1}.$$

It can easily be shown that the wave equation is a Friedrichs system. We consider the case with $c = 2$ and boundary conditions

$$u_1 = 0 \qquad \text{and} \qquad u_2 = c\mathrm{e}^{-100(x_1 - \frac{1}{2})^2}$$

for $x_2 = 0$, $0 \le x_1 \le 1$, and non-reflecting characteristic boundary conditions when $x_1 = 0$ and $x_1 = 1$. Table 7 shows second-order convergence of

Table 7. $||e_h||_0$ and $||e^{\mathrm{trans}}||_0$ for Example 3

Mesh	$\|e_h\|_0$	k	$\|e^{\mathrm{trans}}\|_0$	k
17×17	3.457×10^{-2}	-	3.717×10^{-2}	-
33×33	1.104×10^{-2}	1.65	1.195×10^{-2}	1.64
65×65	2.884×10^{-3}	1.94	3.139×10^{-3}	1.93
129×129	7.261×10^{-4}	1.99	7.917×10^{-4}	1.99
257×257	1.818×10^{-4}	2.00	1.983×10^{-4}	2.00

Table 8. $|||e^{\mathrm{cell}}|||$ and $\bar{\epsilon}_1$ for Example 3

Mesh	$\|\|\|e^{\mathrm{cell}}\|\|\|$	k	$\bar{\epsilon}_1$	k	θ_1
17×17	1.869×10^{-1}	-	2.642×10^{-1}	-	1.41
33×33	1.041×10^{-1}	0.84	1.472×10^{-1}	0.84	1.41
65×65	5.315×10^{-2}	0.97	7.516×10^{-2}	0.97	1.41
129×129	2.667×10^{-2}	1.00	3.772×10^{-2}	0.99	1.41
257×257	1.335×10^{-2}	1.00	1.887×10^{-2}	1.00	1.41

Table 9. $\|e^{\mathrm{cell}}\|_0$ and $\bar{\epsilon}_2$ for Example 3

Mesh	$\|e^{\mathrm{cell}}\|_0$	k	$\bar{\epsilon}_2$	k	θ_2
17×17	3.683×10^{-3}	-	3.753×10^{-3}	-	1.02
33×33	1.026×10^{-3}	1.84	1.043×10^{-3}	1.85	1.02
65×65	2.619×10^{-4}	1.97	2.663×10^{-4}	1.97	1.02
129×129	6.571×10^{-5}	1.99	6.680×10^{-5}	2.00	1.02
257×257	1.644×10^{-5}	2.00	1.671×10^{-5}	2.00	1.02

$||e_h||_0$ and $||e^{\mathrm{trans}}||_0$ – the expected rate of convergence for a smooth solution. Plots of $||e_h||_{0,\kappa}$ and $||e^{\mathrm{trans}}||_{0,\kappa}$ in Figs. 3(a) and (b), respectively, show both errors increasing linearly along characteristic paths from the initial data. Table 8 shows that $|||e^{\mathrm{cell}}|||$ and $\bar{\epsilon}_1$ converge as $O(h)$. As with the previous examples, the error estimate slightly overestimates the error; the graph norm of the cell error does not increase from the inflow of the domain to the outflow and is almost constant along characteristic paths. This suggests that a constant error is being generated in these directions. Finally, the values of $||e^{\mathrm{cell}}||_0$ and $\bar{\epsilon}_2$ in Table 9 are seen to converge as $O(h^2)$, and the error estimate slightly overestimates the error. Figs. 3(e) and (f) show that the distribution of $||e^{\mathrm{cell}}||_{0,\kappa}$ is very similar to $\bar{\epsilon}_2(\kappa)$. Mesh adaptation based on $\bar{\epsilon}_2(\kappa)$ or $\bar{\epsilon}_3(\kappa)$ will direct attention to where the error is being generated, rather than places to which it has been propagated.

5.6. Example 4

In this final example we turn our attention to the streamline-diffusion method on triangular meshes in two-dimensions. In this section we consider a scalar advection problem, based on a combination of Examples 1 and 2. Here, we let

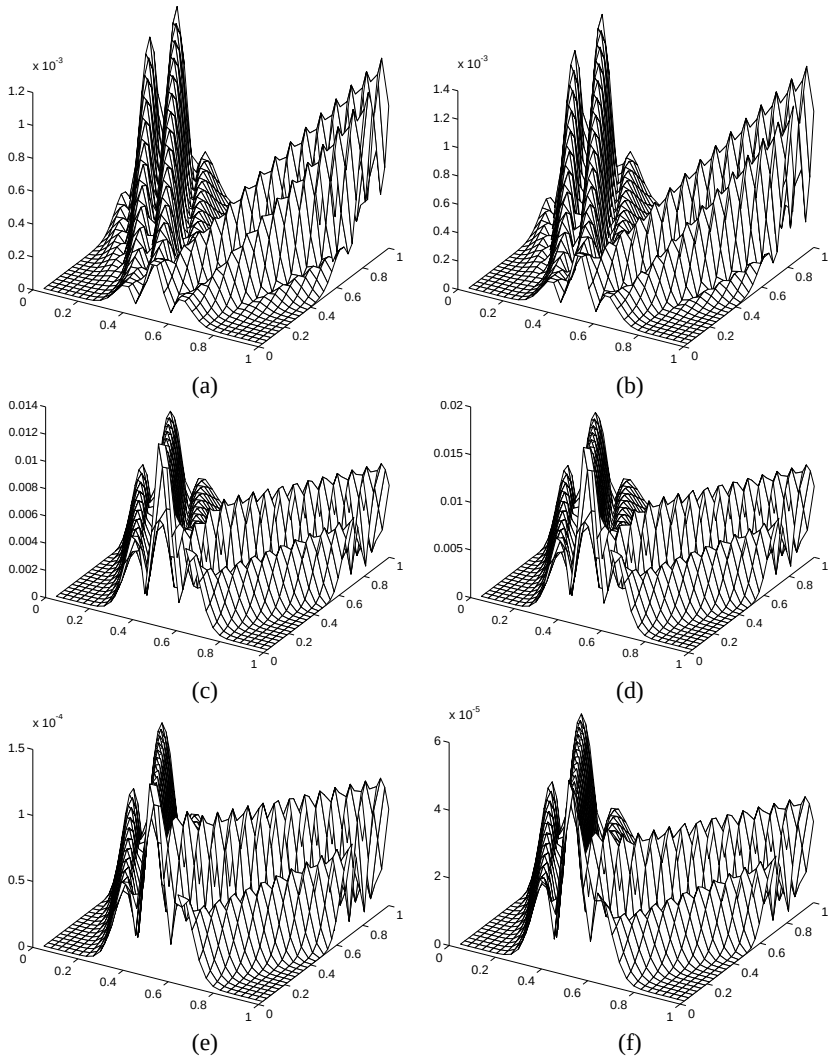

Fig. 3. Example 3: (a) $\|\boldsymbol{e}_h\|_{0,\kappa}$; (b) $\|\boldsymbol{e}^{\mathrm{trans}}\|_{0,\kappa}$; (c) $|||\boldsymbol{e}^{\mathrm{cell}}|||_{\kappa}$; (d) $\bar{\epsilon}_1(\kappa)$; (e) $||\boldsymbol{e}^{\mathrm{cell}}||_{0,\kappa}$; (f) $\bar{\epsilon}_2(\kappa)$

the forcing function $f = 0$, with advective velocity $\boldsymbol{a} = (0.1+\sin(\pi x_2), 2)^{\mathrm{T}}$ and boundary conditions

$$u(x_1, 0) = \begin{cases} \mathrm{e}^{-300(0.4-x_1)^4} & \text{for } 0.0 \le x_1 \le 0.4, \\ 1 & \text{for } 0.4 \le x_1 \le 0.6, \\ 0 & \text{for } 0.6 < x_1 \le 1.0, \end{cases}$$

with a compatible condition along $x_1 = 0$, $0 \le x_2 \le 1$. Throughout this section we set the streamline-diffusion parameter $\delta|_\kappa = 0.5h_\kappa/|\bar{\boldsymbol{a}}_\kappa|$, where

Table 10. $||\boldsymbol{e}_h||_0$ and $||\boldsymbol{e}^{\mathrm{trans}}||_0$ for Example 4

Mesh	$\|\boldsymbol{e}_h\|_0$	k	$\|\boldsymbol{e}^{\mathrm{trans}}\|_0$	k
17×17	1.046×10^{-1}	-	1.007×10^{-1}	-
33×33	8.428×10^{-2}	0.31	8.252×10^{-2}	0.29
65×65	5.915×10^{-2}	0.51	5.747×10^{-2}	0.52
129×129	4.827×10^{-2}	0.29	4.732×10^{-2}	0.28
257×257	3.464×10^{-2}	0.48	3.398×10^{-2}	0.48

Table 11. $\|\boldsymbol{e}^{\mathrm{cell}}\|_0$ and $\bar{\epsilon}_3$ for Example 4

Mesh	$\|\boldsymbol{e}^{\mathrm{cell}}\|_0$	k	$\bar{\epsilon}_3$	k	θ_3
17×17	9.490×10^{-3}	-	2.419×10^{-1}	-	25.5
33×33	5.051×10^{-3}	0.91	1.262×10^{-1}	0.94	25.0
65×65	2.802×10^{-3}	0.85	6.935×10^{-2}	0.86	24.8
129×129	1.566×10^{-3}	0.84	3.857×10^{-2}	0.85	24.6
257×257	8.748×10^{-4}	0.84	2.150×10^{-2}	0.84	24.6

$h_\kappa = \mathrm{diam}(\kappa)$, $\bar{\boldsymbol{a}}_\kappa$ denotes the average of $\boldsymbol{a}$ on element κ and $|\bar{\boldsymbol{a}}_\kappa|$ the Euclidean norm of $\bar{\boldsymbol{a}}_\kappa$.

We first investigate the asymptotic behaviour of the different components of the error using a sequence of uniform triangular meshes: in each case the mesh is constructed from a uniform $N \times N$ mesh by connecting the bottom-left corner of each mesh-square with its top-right corner. In Table 10 we show $||\boldsymbol{e}_h||_0$ and $||\boldsymbol{e}^{\mathrm{trans}}||_0$, along with their respective rates of convergence k. We observe that while the convergence rates for both of these quantities are very similar, in each case k oscillates between $k \sim 0.3$ and $k \sim 0.5$. This behaviour is attributed to the fact that for each of the meshes used, there is not a nodal mesh point where the discontinuity enters the domain. Indeed, numerical experiments based on successively finer uniform meshes which have a mesh point at $x_1 = 0.6, x_2 = 0$, lead to a uniform convergence rate of $k \sim 0.46$ for both $\|\boldsymbol{e}_h\|_0$ and $\|\boldsymbol{e}^{\mathrm{trans}}\|_0$. Table 11 shows $\|\boldsymbol{e}^{\mathrm{cell}}\|_0$, the a posteriori error indicator $\bar{\epsilon}_3$ and the associated effectivity index $\theta_3 = \bar{\epsilon}_3 / \|\boldsymbol{e}^{\mathrm{cell}}\|_0$. In contrast to the convergence rates presented in Table 10, we see that both $\|\boldsymbol{e}^{\mathrm{cell}}\|_0$ and $\bar{\epsilon}_3$ converge at a uniform rate with an effectivity index $\theta_3 \sim 25$. We note that the same asymptotic behaviour is observed for a sequence of meshes which contain a nodal mesh point where the discontinuity enters the domain.

Finally, in Table 12 we present the sequence of meshes generated by the adaptive algorithm described in Sect. 5.2 for TOL $= 0.025$; here $\mathcal{T}_1$ is taken to be a 17×17 uniform triangular mesh constructed as above. We see that each of the components of the error decrease as the adaptive algorithm proceeds; although on the second mesh $\|\boldsymbol{e}^{\mathrm{cell}}\|_0$ has increased slightly. Moreover, we observe that $\bar{\epsilon}_3$ remains an overestimate of the cell error with a constant effectivity index $\theta_3 \sim 20$ on these adaptively refined

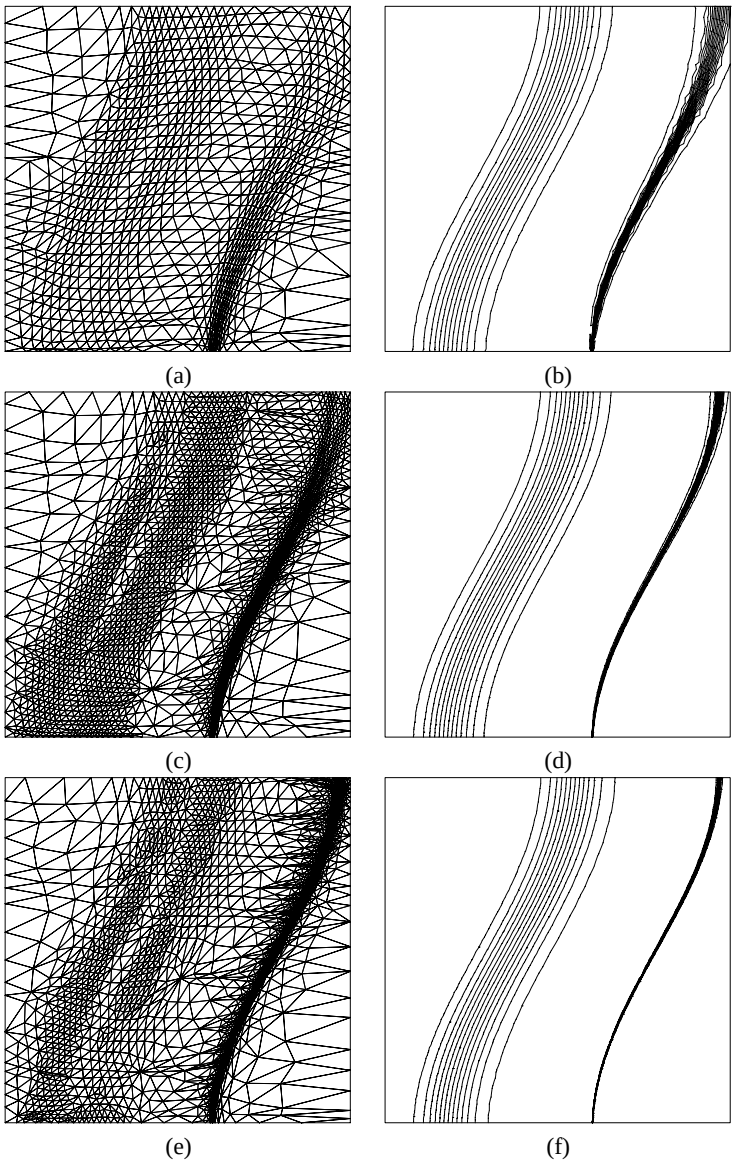

Fig. 4. Example 4: (a) and (b) Mesh (No. 4) and solution, resp., with 949 nodes and 1794 elements; (c) and (d) Mesh (No. 6) and solution, resp., with 2285 nodes and 4451 elements; (e) and (f) Mesh (No. 8) and solution, resp., with 2964 nodes and 5804 elements

meshes. In Fig. 4 we show meshes 4, 6 and 8, along with the corresponding numerical solutions. Here we see that the mesh is concentrated mostly where the discontinuity is located, though the adaptive algorithm has clearly refined the mesh along the top and bottom of the smooth layer also. In particular,

Table 12. Adaptive algorithm for Example 4 with TOL $= 0.025$

Mesh	Nodes	$\|e_h\|_0$	$\|e^{\mathrm{trans}}\|_0$	$\|e^{\mathrm{cell}}\|_0$	$\bar{\epsilon}_3$	θ_3
1	289	1.046×10^{-1}	1.007×10^{-1}	9.490×10^{-3}	2.419×10^{-1}	25.5
2	289	9.380×10^{-2}	8.932×10^{-2}	1.030×10^{-2}	2.358×10^{-1}	22.9
3	949	7.079×10^{-2}	6.779×10^{-2}	6.100×10^{-3}	1.394×10^{-1}	22.8
4	949	5.233×10^{-2}	4.973×10^{-2}	5.181×10^{-3}	1.095×10^{-1}	21.1
5	2285	4.127×10^{-2}	3.945×10^{-2}	3.088×10^{-3}	6.626×10^{-2}	21.5
6	2285	2.838×10^{-2}	2.715×10^{-2}	2.438×10^{-3}	4.877×10^{-2}	20.0
7	2964	2.288×10^{-2}	2.209×10^{-2}	1.554×10^{-3}	3.227×10^{-2}	20.8
8	2964	1.746×10^{-2}	1.683×10^{-2}	1.106×10^{-3}	2.264×10^{-2}	20.5

we note that the adaptive algorithm first concentrates the mesh in the region of the discontinuity closest to the inflow boundary, before refining near the outflow boundary. This is clearly what we would expect based on the surface plots presented in Example 2 for the cell vertex method. This example highlights the accuracy that may be achieved by employing an hr-refinement strategy; the numerical solution in Fig. 4(f) shows how well the discontinuity has been captured, though some numerical diffusion is observable near the outflow boundary.

6. Conclusions

In this paper we have derived residual-based two-sided a posteriori bounds for the locally generated error component in a general class of discretisation methods for Friedrichs systems. To obtain sharp two-sided bounds, we have made extensive use of the graph norm and its dual. We decomposed the global error into a locally created part that is directly related to the local residual on a cell, and a part that is due to transported error from outside the cell. We also derived further upper and lower bounds on the dual graph norm in terms of the L_2 norm of $h\boldsymbol{r}_h$. These results provide a mathematical foundation for the commonly used concept that controlling the local residual may be considered as a device for reducing the local generation of error in adaptive algorithms for hyperbolic problems.

The theoretical framework developed here has been used to derive local error indicators for the Euler equations of compressible gas dynamics in [24]. Future studies will be directed towards a quantitative assessment of the a posteriori error estimates for elliptic and mixed-type systems.

References

1. Adams, R.A. (1975): Sobolev Spaces. Academic Press, New York – San Francisco – London
2. Babuška, I., Rheinboldt, W.C. (1978): Error estimates for adaptive finite element computations. SIAM J. Numer. Anal. **15**, 736–754
3. Balland, P., Süli, E. (1997): Analysis of the cell vertex finite volume method for hyperbolic problems with variable coefficients. SIAM J. Numer. Anal. **34**, 1127–1151
4. Bank, R.E. (1985): PLTMG user's guide. Technical Report Edition 4, University of California, San Diego
5. Friedrichs, K.O. (1958): Symmetric positive linear differential equations. Commun. Pure Appl. Math. **11**, 333–418
6. Göhner, U., Warnecke, G. (1995): A second order finite difference error indicator for adaptive transonic flow computations. Numer. Math. **70**, 129–161
7. Hairer, E., Nørsett, S.P., Wanner, G. (1987): Solving Ordinary Differential Equations I – Nonstiff Problems. Springer-Verlag, Berlin – Heidelberg – New York
8. Hubbard, M.E., Baines, M.J. (1995): Multidimensional upwinding and grid adaptation. In: Morton, K.W., Baines, M.J. (eds.) Numerical Methods for Fluid Dynamics V, pp. 431–437. Clarendon Press, Oxford
9. Johnson, C. (1990): Adaptive finite element methods for diffusion and convection problems. Comput. Methods Appl. Mech. Engrg. **82**, 301–322
10. Johnson, C. (1994): A new paradigm for adaptive finite element methods. In: Whiteman, J.R. (ed.) The Mathematics of Finite Elements and Applications. Highlights 1993, pp. 105–120. John Wiley & Sons, Chichester
11. Johnson, C., Hansbo, P. (1992): Adaptive finite element methods in computational mechanics. Comput. Methods Appl. Mech. Engrg. **101**, 143–181
12. Johnson, C., Nävert, U., Pitkäranta, J. (1984): Finite element methods for linear hyperbolic problems. Comput. Methods Appl. Mech. Engrg. **45**, 285–312
13. Johnson, C., Szepessy, A. (1995): Adaptive finite element methods for conservation laws. Commun. Pure Appl. Math. **48**, 199–243
14. Lax, P.D. (1955): On Cauchy's problem for hyperbolic equations and the differentiability of solutions of elliptic problems. Commun. Pure Appl. Math. **8**, 615–633
15. Lax, P.D., Phillips, R.S. (1960): Local boundary conditions for dissipative symmetric linear differential operators. Commun. Pure Appl. Math. **13**, 427–455
16. Mackenzie, J. (1998): The efficient generation of simple two-dimensional adaptive grids. SIAM J. Sci. Comp. **19**, 1340–1365
17. Mackenzie, J., Sonar, T., Süli, E. (1994): Adaptive finite volume methods for hyperbolic problems. In: Whiteman, J.R. (ed.) The Mathematics of Finite Elements and Applications. Highlights 1993, pp. 289–298. John Wiley & Sons, Chichester
18. Mackenzie, J., Süli, E., Warnecke, G. (1993/94): A posteriori error estimates for the cell-vertex finite volume method. In: Hackbusch, W., Wittum, G. (eds.) Adaptive Methods: Algorithms, Theory and Applications, Vol. 44, pp. 221–235. Vieweg, Braunschweig
19. Morton, K.W., Süli, E. (1991): Finite volume methods and their analysis. IMA J. Numer. Anal. **11**, 241–260
20. Morton, K.W., Süli, E. (1994): A posteriori and a priori error analysis of finite volume methods. In: Whiteman, J.R. (ed.) The Mathematics of Finite Elements and Applications. Highlights 1993, pp. 267–288. John Wiley & Sons, Chichester
21. Nečas, J. (1967): Les Méthodes Directes en Théorie des Équations Elliptiques. Masson, Paris

22. Rheinhardt, H.J. (1981): A posteriori error estimates for the finite element solution of singularly perturbed linear ordinary differential equation. SIAM J. Numer. Anal. **18**, 406–430
23. Sonar, T. (1993): Strong and weak norm error indicators based on the finite element residual for compressible flow computations. Impact Comp. Sci. Engrg. **5**, 111–127
24. Sonar, T., Süli, E. (1998): A dual graph-norm refinement indicator for finite volume approximations of the Euler equations. Numerische Mathematik **78**, 619–658
25. Süli, E. (1989): Finite volume methods on distorted meshes: stability, accuracy, adaptivity. Technical Report NA89/6, Oxford University Computing Laboratory
26. Süli, E. (1992): The accuracy of cell vertex finite volume methods on quadrilateral meshes. Math. Comp. **59**, 359–382
27. Süli, E. (1991): The accuracy of finite volume methods on distorted partitions. In: Whiteman, J.R. (ed.) The Mathematics of Finite Elements and Applications VII, pp. 253–260. Academic Press, London
28. Süli, E. (1991): Convergence of finite volume schemes for Poisson's equation on nonuniform meshes. SIAM J. Numer. Anal. **28**, 1419–1430
29. Süli, E. (1996): A posteriori error analysis and global error control for adaptive finite element approximations of hyperbolic problems. In: Griffiths, D.F., Watson, G.A. (eds.) Numerical Analysis, Pitman Research Notes in Mathematics Series **344**, pp. 169–190. Longman Scientific and Technical, Harlow
30. Süli, E. (1997): A posteriori error analysis and adaptivity for finite element approximations of hyperbolic problems. In: Kröner, D., Ohlberger, M., Rohde, C. (eds.) An introduction to recent developments in theory and numerics of conservation laws, pp. 123–194. Springer, Berlin
31. Süli, E., Houston, P. (1997): Finite element methods for hyperbolic problems: a posteriori error analysis and adaptivity. In: Duff, I. and Watson G.A. (eds.) State of the Art in Numerical Analysis, pp. 441–471. Oxford University Press, Oxford
32. Taylor, M. (1981): Pseudodifferential Operators. Princeton Univ. Press, Princeton, New Jersey